Part I

The Genesis Framework

Chapter 1

Genesis Framework: Cosmological Unification

1.1 Introduction to the Genesis Framework

The [G] Framework emerges from a fundamentally different paradigm than the Aether Framework presented in Chapters **??**–**??**. While Aether describes spacetime as a continuous crystalline lattice with scalar field-ZPE coupling at laboratory scales, Genesis proposes:

- **Nodespace**: A discrete network of universal nodes as the substrate of reality
- **Origami Dimensions**: Dimensional folding mechanisms enabling continuous transitions between fractal and integer dimensions
- **Meta-Principle Superforce**: A governing organizational framework transcending standard force unification
- **Cosmological Scale**: Predictions testable via CMB, large-scale structure, and gravitational waves

The Genesis Framework views mathematics as the universal language of reality, where symmetry, fractal self-similarity, and higher-dimensional structures are not abstract concepts but the fundamental building blocks of existence.

1.1.1 Philosophical Foundations

Mathematics as Universal Language Genesis begins with the premise that mathematical structures–exceptional Lie algebras (E_8), Cayley-Dickson constructions, modular forms–are not merely descriptive tools but constitutive elements of physical reality. The universe is a "fractal symphony" [G], where patterns at Planck scales mirror structures in cosmic microwave background radiation.

Emergence from Symmetry Breaking Consider an infinite, perfect E_8 lattice stretching across dimensions. Small perturbations, analogous to quantum fluctuations, disrupt this perfection. These disturbances cascade through dimensions, generating fractal harmonics and giving birth to forces, particles, and spacetime itself.

The Genesis paradigm asserts that complexity emerges from simplicity through recursive dynamics:

$$\mathcal{F}_{\text{cosmos}}(x,t) = \sum_{n=0}^{\infty} \beta^n F^n(x) \qquad \text{[G:COSMO:T]}$$

where $F^n(x)$ represents fractal layers nested hierarchically, and $\beta < 1$ ensures convergence. Each layer encodes structure at a different scale, from subatomic to galactic.

1.1.2 Genesis vs Aether: Paradigm Comparison

Table **??** contrasts the two frameworks:

Table 1.1: Comparison of Genesis and Aether Frameworks

Aspect	**Aether**	**Genesis**
Substrate	Continuous crystalline lattice	Discrete nodespace network
Dimensions	Integer (via Cayley-Dickson)	Fractal/origami (continuous folding)
Unification	Scalar-ZPE coupling	Meta-Principle Superforce
Scale	Planck $\rightarrow$ lab (Casimir, spectroscopy)	Cosmological (CMB, LSS, GW)
Testability	$\pm 15\%$ Casimir, $\pm 12\%$ vibr.	Low-l CMB, fractal LSS
Philosophy	Emergent from lattice vibrations	Emergent from symmetry breaking

1.1.3 Roadmap to Chapters 12–14

This chapter provides an overview. Subsequent chapters develop:

- **Chapter ??**: Nodespace topology, connectivity, emergence of spacetime
- **Chapter ??**: Dimensional folding, fractal dimensions, cosmological signatures
- **Chapter ??**: Meta-Principle Lagrangian, force unification, experimental tests

1.2 Nodespace: The Universal Substrate

1.2.1 Nodespace as Discrete Network

Genesis proposes that spacetime is not fundamentally continuous. Instead, reality consists of a *nodespace* [G]–a network of discrete nodes connected by relationships. Spacetime emerges from the topological structure of this network.

Graph-Theoretic Formulation Nodespace is modeled as a graph $\mathcal{N} = (V, E)$ where:

- $V = \{v_i\}$ is the set of nodes (fundamental units of existence)
- $E = \{(v_i, v_j)\}$ is the set of edges (relationships between nodes)

The *graph distance* $d_{\text{graph}}(i,j)$ is the length of the shortest path between nodes i and j. This discrete metric replaces the continuous Euclidean distance in standard spacetime.

1.2.2 Connectivity Matrix

Node interactions are quantified by the *connectivity matrix*:

$$C_{ij} = \exp\left(-\frac{d_{\text{graph}}(i,j)}{\lambda_{\text{node}}}\right) \quad \text{[G:TOPO:T]}$$

where λ_{node} is the *nodespace lattice constant*, estimated to be:

$$\lambda_{\text{node}} \sim 10^{-15}\ \text{m} \approx 10^3 l_{\text{Planck}} \quad \text{[G:TOPO:S]}$$

This is slightly larger than the Planck length, suggesting nodespace structure emerges from pre-geometric quantum foam.

Physical Interpretation C_{ij} quantifies the "strength of connection" between nodes. High connectivity ($C_{ij} \to 1$) indicates nodes are closely related; low connectivity ($C_{ij} \to 0$) indicates isolation. The exponential form ensures that:

1. Nearby nodes ($d_{\text{graph}} \ll \lambda_{\text{node}}$) are strongly connected
2. Distant nodes ($d_{\text{graph}} \gg \lambda_{\text{node}}$) are effectively decoupled
3. Connectivity decays smoothly, preventing discontinuities

1.2.3 Emergence of Spacetime

The metric tensor $g_{\mu\nu}$ emerges from nodespace structure:

$$g_{\mu\nu}(x) \sim \mathcal{F}[C_{ij}] \quad \text{[G:GR:S]}$$

where $\mathcal{F}$ is a functional mapping connectivity to geometry. In the continuum limit ($\lambda_{\text{node}} \to 0$, $N_{\text{nodes}} \to \infty$), this reproduces general relativity.

Nodespace Lagrangian The action for nodespace dynamics:

$$S_{\text{nodespace}} = \int d^n x \sqrt{-g}\, \mathcal{F}(x, t, D, z) \quad \text{[G:GR:T]}$$

where $\mathcal{F}$ integrates nodespace connectivity, fractal corrections, and modular symmetries.

1.3 Meta-Principle Superforce: Beyond Standard Forces

1.3.1 The Superforce Concept

The Genesis *Meta-Principle Superforce* [G] is not a fifth force in the traditional sense. It is an organizing framework that governs:

- The structure of nodespace
- Dimensional folding dynamics
- The hierarchical emergence of standard forces (gravity, EM, weak, strong)
- Cosmological evolution and multiverse resonance

Philosophical Distinction Traditional force unification (Grand Unified Theories, String Theory) seeks to merge forces at high energies into a single gauge group. The Superforce operates differently: it is the *meta-structure* from which forces emerge through symmetry breaking and dimensional projection.

1.3.2 Superforce Potential

The Meta-Principle potential governs field configurations:

$$V_{\text{MP}}(\phi, \chi) = \alpha\phi^2 + \beta\chi^4 + \gamma\phi\chi^2 + \Delta_{\text{MP}} \quad \text{[G:COSMO:T]}$$

where:

- ϕ: Meta-principle scalar field (distinct from Aether's ϕ_{Aether})
- χ: Origami folding parameter (encodes dimensional state)
- α, β, γ: Coupling constants
- Δ_{MP}: Meta-principle correction term (non-polynomial)

Coupling Constants Typical values:

$$\alpha \sim 10^{-2}\ M_{\text{Pl}}^2 \quad \text{[G:COSMO:S]}$$
$$\beta \sim 10^{-4}\ M_{\text{Pl}}^{-2} \quad \text{[G:COSMO:S]}$$
$$\gamma \sim 10^{-3}\ M_{\text{Pl}}^0 \quad \text{[G:COSMO:S]}$$

1.3.3 Force Emergence

Standard forces emerge as projections of the Superforce onto different nodespace sectors:

$$\mathcal{F}_{\text{standard}} = \mathcal{P}_{\text{sector}}\left[\mathcal{F}_{\text{Superforce}}\right] \quad \text{[G:COSMO:T]}$$

where $\mathcal{P}_{\text{sector}}$ is a projection operator onto gauge groups.

1.4 Observer-Dependent Reality

1.4.1 Observer Wavefunction

Genesis incorporates the observer into the fundamental formalism. The *observer wavefunction*:

$$\Psi_{\text{observer}} = \sum_k c_k \left|\text{nodespace}_k\right\rangle \quad \text{[G:QM:S]}$$

represents a superposition of possible nodespace configurations. Measurement collapses this into a specific observed reality.

1.4.2 Consciousness as Resonance

Genesis posits that consciousness emerges as a *resonance phenomenon* within nodespace:

$$C(x,t) = \int \mathcal{G}(x,t,D,z) \cdot e^{i\nu t}\, dx \quad \text{[G:QM:S]}$$

where $C(x,t)$ is the consciousness field and ν is the resonance frequency.

Speculative Nature We acknowledge Eq. **??** as highly speculative. Experimental validation requires understanding neural correlates of consciousness and testing for non-local resonance effects.

1.5 The Genesis Master Equation

1.5.1 Unified Formulation

The Genesis Framework culminates in the *Genesis Master Equation*:

$$\mathcal{G}(x,t,D,z) = \sum_{n=0}^{\infty} \beta^n F^n(x) + \int \frac{d^\alpha x}{dt^\alpha} D_f(D_n) + \mathcal{R}(z) + V_{\text{MP}}(\phi,\chi) \quad \text{[G:COSMO:T]}$$

where:

- $F^n(x)$: Recursive fractal dynamics at layer n
- $\frac{d^\alpha x}{dt^\alpha}$: Fractional time derivative (fractional order α)
- $D_f(D_n)$: Fractional and negative-dimensional contributions
- $\mathcal{R}(z)$: Modular symmetries governing periodic harmonies
- V_{MP}: Meta-principle potential

1.5.2 Fractal Dynamics Term

The recursive fractal term:

$$F^n(x) = \frac{1}{\phi^n} \cos\left(\phi^n \frac{x}{x_0}\right) \quad \text{[G:MATH:T]}$$

where $\phi = (1+\sqrt{5})/2$ is the golden ratio.

1.5.3 Fractional Time Evolution

The fractional derivative encodes non-local temporal correlations:

$$\frac{d^\alpha x}{dt^\alpha} = \frac{1}{\Gamma(1-\alpha)} \frac{d}{dt} \int_0^t \frac{x(s)}{(t-s)^\alpha}\, ds \quad \text{[G:MATH:T]}$$

1.6 Experimental Signatures

1.6.1 Cosmological Observables

Genesis makes predictions testable with cosmological observations:

1. **CMB Angular Power Spectrum**: Low-l suppression ($l < 30$)

$$C_l^{\text{Genesis}} = C_l^{\text{LCDM}} \cdot \left(1 - \epsilon \cdot e^{-l/l_0}\right) \quad \text{[G:EXP:E]}$$

where $\epsilon \sim 0.1$ and $l_0 \sim 20$.

2. **Large-Scale Structure**: Fractal dimension $d_f \approx 2.2$–2.4

$$N(r) \sim r^{d_f}, \quad d_f = 2 + \delta_{\text{fractal}} \tag{G:EXP:E}$$

3. **Gravitational Waves**: Subtle strain modifications

$$h_{\mu\nu}^{\text{Genesis}} = h_{\mu\nu}^{\text{GR}} + \delta h_{\mu\nu}(\phi_{\text{MP}}) \tag{G:EXP:S}$$

1.7 Worked Examples

Example 1.1 (Nodespace Connectivity Calculation)**. Problem:** A nodespace network has 100 nodes with average degree $\langle k \rangle = 6$. Calculate the total number of edges E, the connectivity density $\rho_c = E/E_{\max}$, and estimate the critical percolation threshold p_c for dimensional emergence.

Solution:

For undirected graph with $N = 100$ nodes and average degree $\langle k \rangle = 6$:

Total edges (each edge counted once):

$$E = \frac{N\langle k \rangle}{2} = \frac{100 \times 6}{2} = 300 \tag{1.1}$$

Maximum possible edges (complete graph):

$$E_{\max} = \frac{N(N-1)}{2} = \frac{100 \times 99}{2} = 4950 \tag{1.2}$$

Connectivity density:

$$\rho_c = \frac{E}{E_{\max}} = \frac{300}{4950} = 0.0606 \approx 6\% \tag{1.3}$$

For random graphs, percolation threshold (Erdos-Renyi):

$$p_c = \frac{\langle k \rangle}{N-1} = \frac{6}{99} = 0.0606 \tag{1.4}$$

At current connectivity $\rho_c = p_c$, system is exactly at critical point for dimensional emergence.

Result: Network has 300 edges, 6% density, and sits at percolation threshold.

Physical Interpretation: Genesis framework requires nodespace to be just above percolation threshold for spacetime to emerge while maintaining quantum foam fluctuations. This critical connectivity balances macroscopic coherence with microscopic uncertainty.

Example 1.2 (Meta-Principle Superforce Strength)**. Problem:** Estimate the Meta-Principle Superforce coupling strength α_{MP} at energy scale $E = 10^{16}\,\text{GeV}$ (GUT scale) using the relation $\alpha_{\text{MP}}(E) = \alpha_0 \cdot (E/M_{\text{Pl}})^{\beta}$ with $\alpha_0 = 1$ (dimensionless unification strength) and $\beta = 0.3$ (anomalous dimension). Compare to electromagnetic fine structure constant $\alpha_{\text{EM}} \approx 1/137$.

Solution:

Planck mass: $M_{\text{Pl}} = 1.22 \times 10^{19}\,\text{GeV}$

Energy ratio:

$$\frac{E}{M_{\text{Pl}}} = \frac{10^{16}\,\text{GeV}}{1.22 \times 10^{19}\,\text{GeV}} = 8.2 \times 10^{-4} \tag{1.5}$$

Superforce coupling:

$$\alpha_{\text{MP}}(E) = 1 \times (8.2 \times 10^{-4})^{0.3} \tag{1.6}$$

Compute exponent:

$$\ln[\alpha_{\text{MP}}] = 0.3 \times \ln\left(8.2 \times 10^{-4}\right) = 0.3 \times (-7.107) = -2.132 \tag{1.7}$$

$$\alpha_{\text{MP}} = e^{-2.132} = 0.119 \tag{1.8}$$

Ratio to electromagnetism:

$$\frac{\alpha_{\text{MP}}}{\alpha_{\text{EM}}} = \frac{0.119}{1/137} = 0.119 \times 137 = 16.3 \tag{1.9}$$

Result: Superforce coupling $\alpha_{\text{MP}} \approx 0.12$ at GUT scale, 16× stronger than electromagnetism.

Physical Interpretation: Meta-Principle Superforce becomes strong at high energies, unifying all forces. At low energies ($E \ll M_{\text{Pl}}$), $\alpha_{\text{MP}} \to 0$, explaining why we observe force splitting in experiments.

Example 1.3 (CMB Low-l Suppression Prediction)**. Problem:** Using Genesis prediction $C_l^{\text{Genesis}} = C_l^{\text{LCDM}} \cdot (1 - \epsilon e^{-l/l_0})$ with $\epsilon = 0.1$ and $l_0 = 20$, calculate the fractional suppression at multipoles $l = 2, 10, 30, 100$. Compare to Planck satellite measurement precision ($\sim 1\%$ at low l).

Solution:

Suppression factor: $S(l) = 1 - \epsilon e^{-l/l_0}$

At $l = 2$:

$$S(2) = 1 - 0.1 \times e^{-2/20} = 1 - 0.1 \times e^{-0.1} = 1 - 0.1 \times 0.905 = 1 - 0.0905 = 0.910 \tag{1.10}$$

Fractional suppression: $1 - S(2) = 9.0\%$

At $l = 10$:

$$S(10) = 1 - 0.1 \times e^{-10/20} = 1 - 0.1 \times e^{-0.5} = 1 - 0.1 \times 0.607 = 0.939 \tag{1.11}$$

Fractional suppression: 6.1%

At $l = 30$:

$$S(30) = 1 - 0.1 \times e^{-30/20} = 1 - 0.1 \times e^{-1.5} = 1 - 0.1 \times 0.223 = 0.978 \tag{1.12}$$

Fractional suppression: 2.2%

At $l = 100$:

$$S(100) = 1 - 0.1 \times e^{-100/20} = 1 - 0.1 \times e^{-5} = 1 - 0.1 \times 0.0067 = 0.9993 \tag{1.13}$$

Fractional suppression: 0.07%

Result: Genesis predicts 9% suppression at $l = 2$, decaying to $< 0.1\%$ by $l = 100$.

Physical Interpretation: Planck satellite measures CMB at 1% precision for low l, making the predicted 9% ($l = 2$) and 6% ($l = 10$) suppressions potentially observable. Current data shows mild low-l anomalies, though not definitively confirming Genesis. Future high-precision missions may resolve this.

1.8 Summary and Forward Look

1.8.1 Chapter Summary

This chapter introduced the Genesis Framework:

- **Nodespace**: Discrete network substrate with connectivity matrix C_{ij}
- **Meta-Principle Superforce**: Organizing framework governing force emergence
- **Genesis Master Equation**: Unified formulation integrating fractals, dimensions, modular symmetries
- **Cosmological Predictions**: CMB low-l suppression, fractal LSS, GW modifications

1.8.2 Integration with Aether

Genesis complements Aether at different scales:

- **Aether**: Continuous lattice, lab-scale, scalar-ZPE coupling
- **Genesis**: Discrete nodespace, cosmological scale, Meta-Principle Superforce

1.8.3 Next Chapters

- **Chapter ??**: Nodespace topology, graph Laplacian, spacetime emergence
- **Chapter ??**: Dimensional folding operators, fractal dimensions
- **Chapter ??**: Superforce Lagrangian, force unification

Chapter 2

Nodespace Theory: Graph-Theoretic Foundations

2.1 Introduction: Beyond Continuous Spacetime

The [G] Framework challenges a fundamental assumption of general relativity: that spacetime is a smooth, continuous manifold. Instead, Genesis proposes that at the most fundamental level, reality consists of a discrete network–a *nodespace*–from which continuous spacetime emerges as an effective description.

This paradigm shift has profound implications:

- **Discreteness at Planck Scale**: Resolves infinities and divergences plaguing quantum field theory in curved spacetime
- **Graph-Theoretic Structure**: Enables rigorous mathematical treatment via algebraic topology and spectral graph theory
- **Emergent Geometry**: Metric tensor $g_{\mu\nu}$ arises from network connectivity, not imposed *a priori*
- **Quantum-Gravitational Unification**: Nodespace provides natural framework for quantum gravity

2.1.1 Historical Context

Nodespace theory builds on several theoretical predecessors:

1. **Causal Sets** (Sorkin, 1987): Spacetime as partially ordered set with causal structure
2. **Spin Networks** (Penrose, 1971; Rovelli, 1995): Quantum states of geometry as graphs
3. **Loop Quantum Gravity** (Ashtekar, 1986): Area and volume quantized via spin network states
4. **Causal Dynamical Triangulations** (Ambjorn, Loll, 2004): Spacetime from Regge calculus

Genesis nodespace extends these approaches by integrating:

- Fractal-modular symmetries from Monster Group and E_8 lattice

- Meta-Principle Superforce governing network evolution
- Origami dimensional folding connecting nodespace layers

2.2 Graph-Theoretic Formulation of Nodespace

2.2.1 Nodespace as Directed Graph

Formally, nodespace is a *directed graph* $\mathcal{N} = (V, E, w)$ where:

$$\mathcal{N} = (V, E, w) \tag{G:TOPO:T}$$

with components:

- $V = \{v_i\}_{i=1}^{N}$: Set of **nodes** (fundamental units, N possibly infinite)
- $E \subseteq V \times V$: Set of **edges** (relationships, $(v_i, v_j) \in E$ if nodes connected)
- $w : E \to \mathbb{R}^+$: **Weight function** (connection strength)

Physical Interpretation

- **Nodes**: Represent "atoms of spacetime," analogous to Planck-scale events
- **Edges**: Encode causal relationships, quantum entanglement, or information channels
- **Weights**: Quantify interaction strength, modulated by Meta-Principle Superforce

2.2.2 Emergent Potential Field Dynamics

The evolution of nodespace is governed by an emergent potential field that integrates temporal decay, dimensional coherence, and modular symmetries. This potential field determines how node connections strengthen or weaken over time:

$$\Phi_{\text{nodes}}(t, D, z) = \int_0^\infty \frac{e^{-\kappa t}}{(1 + \gamma D^2)^{1/2}}\, dt \tag{G:EM:T}$$

where t is time, D represents dimensional parameters (encoding which compactified dimensions are active), z signifies modular symmetries from the Monster Group (Ch **??**), κ is the decay constant of interactions (governing how quickly connections fade without reinforcement), and γ encodes dimensional coherence (measuring how well dimensions remain coupled). This integral formulation captures the time-evolution of nodespace potentials, with the exponential decay term ensuring causality (future cannot influence past) and the dimensional factor $(1 + \gamma D^2)^{-1/2}$ providing dimensional damping that stabilizes higher-dimensional fluctuations.

2.2.3 Graph Distance and Metric

The *graph distance* $d_{\text{graph}}(i, j)$ is the length of the shortest path between nodes v_i and v_j:

$$d_{\text{graph}}(i, j) = \min \{n \mid \exists \text{ path } v_i = u_0, u_1, \ldots, u_n = v_j\} \tag{G:TOPO:T}$$

If no path exists, $d_{\text{graph}}(i, j) = \infty$. For weighted graphs, path length sums edge weights.

Properties of Graph Distance

1. **Symmetry** (for undirected graphs): $d_{\text{graph}}(i,j) = d_{\text{graph}}(j,i)$
2. **Triangle Inequality**: $d_{\text{graph}}(i,k) \leq d_{\text{graph}}(i,j) + d_{\text{graph}}(j,k)$
3. **Positive Definiteness**: $d_{\text{graph}}(i,j) = 0 \iff i = j$

Thus (V, d_{graph}) forms a metric space in the graph-theoretic sense.

2.2.4 Adjacency and Incidence Matrices

The graph structure is encoded in the *adjacency matrix* A:

$$A_{ij} = \begin{cases} w(v_i, v_j) & \text{if } (v_i, v_j) \in E \\ 0 & \text{otherwise} \end{cases} \quad \text{[G:TOPO:T]}$$

For unweighted graphs, $A_{ij} \in \{0, 1\}$. The adjacency matrix satisfies:

- **Symmetry** (undirected): $A_{ij} = A_{ji}$
- **Zero Diagonal** (no self-loops): $A_{ii} = 0$

Degree Matrix The *degree matrix* D is diagonal:

$$D_{ii} = \sum_{j=1}^{N} A_{ij}, \quad D_{ij} = 0 \text{ for } i \neq j \quad \text{[G:TOPO:T]}$$

D_{ii} counts the number of edges incident to node v_i (or sum of weights for weighted graphs).

2.3 Connectivity Matrix and Exponential Decay

2.3.1 Definition of Connectivity Matrix

The *connectivity matrix* C quantifies the strength of connection between all node pairs, incorporating both direct edges and multi-hop paths:

$$C_{ij} = \exp\left(-\frac{d_{\text{graph}}(i,j)}{\lambda_{\text{node}}}\right) \quad \text{[G:TOPO:T]}$$

where λ_{node} is the *nodespace lattice constant*, the characteristic length scale.

Key Features

1. **Local Connectivity**: For $d_{\text{graph}} \ll \lambda_{\text{node}}$, $C_{ij} \approx 1$ (strong connection)
2. **Long-Range Decay**: For $d_{\text{graph}} \gg \lambda_{\text{node}}$, $C_{ij} \to 0$ exponentially
3. **Smooth Interpolation**: No discontinuities; connectivity decays smoothly with distance
4. **Diagonal Dominance**: $C_{ii} = 1$ (self-connectivity), ensuring matrix regularity

2.3.2 Lattice Constant and Physical Scales

The nodespace lattice constant is estimated from dimensional analysis and quantum gravity considerations:

$$\lambda_{\text{node}} \sim 10^{-15} \text{ m} = 1 \text{ fm} \approx 10^3 \, l_{\text{Planck}} \quad \text{[G:TOPO:S]}$$

This is slightly larger than the Planck length $l_{\text{Planck}} = \sqrt{\hbar G/c^3} \approx 1.6 \times 10^{-35}$ m, suggesting:

- Nodespace emerges from pre-geometric quantum foam at Planck scale
- Effective discreteness becomes apparent at femtometer scale (nuclear physics)
- Continuum limit valid for $\lambda \gg \lambda_{\text{node}}$

Table 2.1: Characteristic Length Scales in Quantum Gravity

Approach	**Scale**	**Value**
Planck length	l_{Planck}	1.6×10^{-35} m
Loop quantum gravity	$\sqrt{\gamma}\, l_{\text{Planck}}$	$\sim 10^{-35}$ m ($\gamma \sim 1$)
String theory	$l_s \sim \alpha' M_s^{-1}$	$\sim 10^{-34}$ m (typical)
Genesis nodespace	λ_{node}	10^{-15} m (this work)

Comparison with Other Quantum Gravity Approaches Genesis nodespace operates at coarser scale than Planck length, potentially making experimental signatures more accessible.

2.3.3 Connectivity Matrix Properties

Matrix Norms and Spectrum The connectivity matrix C is symmetric positive-definite:

Theorem 2.1 (Connectivity Matrix Positivity)**.** *For any nodespace graph $\mathcal{N}$, the connectivity matrix C defined by Eq.* **??** *satisfies:*

1. $C_{ij} = C_{ji}$ *(symmetry)*
2. *All eigenvalues* μ_k *satisfy* $0 < \mu_k \leq 1$
3. $\det(C) > 0$ *(positive-definite)*

Proof. Symmetry follows from graph distance symmetry. Positivity: for any vector $\mathbf{v} \in \mathbb{R}^N$,

$$\mathbf{v}^T C \mathbf{v} = \sum_{i,j} v_i C_{ij} v_j = \sum_{i,j} v_i v_j e^{-d_{ij}/\lambda} > 0$$

since exponential is strictly positive. Eigenvalues bounded by Gershgorin circle theorem. □

2.4 Continuum Limit and Emergence of Spacetime

2.4.1 From Graph to Manifold

As $N \to \infty$ and $\lambda_{\text{node}} \to 0$ (while maintaining $N\lambda_{\text{node}}^d$ constant), nodespace approaches a continuous manifold. This limit is formalized via *graph Laplacian convergence*.

Graph Laplacian The *graph Laplacian* L is defined as:

$$L = D - A \tag{G:MATH:T}$$

For functions $f : V \to \mathbb{R}$ on nodes, the Laplacian acts as:

$$(Lf)_i = \sum_j A_{ij}(f_i - f_j) = D_{ii}f_i - \sum_j A_{ij}f_j \tag{G:MATH:T}$$

Convergence Theorem

Theorem 2.2 (Laplacian Continuum Limit)**.** *As the nodespace graph refines ($N \to \infty$, $\lambda_{node} \to 0$) with nodes uniformly distributed in Euclidean space $\mathbb{R}^d$, the normalized graph Laplacian $\frac{1}{\lambda_{node}^2}L$ converges to the continuum Laplacian:*

$$\frac{1}{\lambda_{node}^2}Lf \to \nabla^2 f = \sum_{\mu=1}^{d} \frac{\partial^2 f}{\partial x^\mu \partial x^\mu} \tag{G:MATH:T}$$

This establishes the rigorous connection between discrete nodespace and continuous spacetime.

2.4.2 Metric Tensor Emergence

The metric tensor $g_{\mu\nu}$ emerges from the connectivity matrix via a functional mapping:

$$g_{\mu\nu}(x) = \mathcal{F}[C_{ij}]\Big|_{x\in\mathcal{M}} \tag{G:GR:S}$$

where $\mathcal{F}$ is a functional that extracts geometric information from network topology.

Explicit Construction (Regge Calculus) One explicit realization uses *Regge calculus*:

1. Assign spacetime coordinates $x^\mu(v_i)$ to each node v_i
2. Define edge lengths $l_{ij} = ||x(v_i) - x(v_j)||$
3. Construct simplicial complex (triangulation) from nodespace graph
4. Metric components emerge from edge length assignments

For details, see Regge (1961) and modern implementations in causal dynamical triangulations (Ambjorn & Loll, 2004).

2.4.3 General Relativity as Emergent Theory

In the continuum limit, Einstein's field equations emerge from nodespace dynamics:

$$R_{\mu\nu} - \frac{1}{2}g_{\mu\nu}R = \frac{8\pi G}{c^4}T_{\mu\nu} \tag{G:GR:T}$$

where:

- $R_{\mu\nu}$: Ricci curvature tensor (from $g_{\mu\nu}$ emerged from C_{ij})
- R: Ricci scalar
- $T_{\mu\nu}$: Stress-energy tensor (from nodespace matter content)

Nodespace Corrections At scales $\lambda \sim \lambda_{\text{node}}$, corrections appear:

$$G_{\mu\nu} = \frac{8\pi G}{c^4} T_{\mu\nu} + \delta G_{\mu\nu}(\lambda_{\text{node}}) \quad \text{[G:GR:S]}$$

where $\delta G_{\mu\nu}$ encodes quantum-gravitational effects from discrete structure.

2.5 Nodespace Dynamics and Evolution

2.5.1 Inter-Nodespace Interactions

Nodespaces interact through *resonant tunneling*, governed by modular transformations. The tunneling amplitude between nodespace configurations z_i and z_j is:

$$T(z_i, z_j) = \exp\left(-\alpha \cdot \frac{|z_i - z_j|}{\lambda_{\text{res}}}\right) \quad \text{[G:TOPO:T]}$$

where:

- $z_i, z_j \in \mathbb{C}$: Modular coordinates of nodespace states
- α: Tunneling suppression factor ($\alpha \sim 1$ for typical configurations)
- λ_{res}: Resonance wavelength ($\lambda_{\text{res}} \sim \lambda_{\text{node}}$)

Modular Transformations Nodespace coordinates transform under modular group $SL(2, \mathbb{Z})$:

$$z \to \frac{az + b}{cz + d}, \quad a, b, c, d \in \mathbb{Z}, \quad ad - bc = 1 \quad \text{[G:MATH:T]}$$

This connects to String Theory's T-duality and Monster Group moonshine.

2.5.2 Nodespace Action and Field Equations

The nodespace action integrates over all nodes and edges:

$$S_{\text{nodespace}} = \int d^n x \, \sqrt{-g} \, \mathcal{F}(x, t, D, z) \quad \text{[G:GR:T]}$$

where $\mathcal{F}$ is the nodespace functional incorporating:

- Connectivity matrix C_{ij}
- Fractal corrections from Meta-Principle
- Modular symmetries $z \in \mathbb{H}$ (upper half-plane)

Variational Principle Extremizing the action with respect to connectivity yields nodespace field equations:

$$\frac{\delta S_{\text{nodespace}}}{\delta C_{ij}} = 0 \implies \Box C_{ij} + V'(C_{ij}) = J_{ij} \quad \text{[G:GR:T]}$$

where:

- $\Box = D - A$: Graph Laplacian operator
- $V(C)$: Effective potential for connectivity
- J_{ij}: Source term from matter/energy distribution

2.5.3 Time Evolution of Nodespace

Nodespace evolves dynamically under Hamiltonian:

$$H_{\text{nodespace}} = \sum_{i,j} \frac{1}{2}\Pi_{ij}^2 + V(C_{ij}) + H_{\text{int}} \quad \text{[G:QM:T]}$$

where:

- $\Pi_{ij} = \frac{\partial C_{ij}}{\partial t}$: Canonical momentum conjugate to C_{ij}
- $V(C)$: Potential energy (from Meta-Principle)
- H_{int}: Interaction term between nodes

Heisenberg Equations of Motion

$$\frac{dC_{ij}}{dt} = \{C_{ij}, H_{\text{nodespace}}\}_{\text{PB}} = \Pi_{ij} \quad \text{[G:QM:T]}$$

$$\frac{d\Pi_{ij}}{dt} = -\frac{\partial V}{\partial C_{ij}} - \sum_k \frac{\partial H_{\text{int}}}{\partial C_{ik}}\delta_{jk} \quad \text{[G:QM:T]}$$

These equations describe the quantum evolution of nodespace connectivity.

2.6 Nodespace Quantum Fluctuations

2.6.1 Vacuum Fluctuations in Nodespace

Even in the absence of classical matter, nodespace exhibits quantum fluctuations. The connectivity matrix fluctuates around its vacuum expectation value:

$$C_{ij}(t) = \langle C_{ij} \rangle + \delta C_{ij}(t) \quad \text{[G:QM:T]}$$

where δC_{ij} represents quantum fluctuations.

Two-Point Correlation Function The fluctuation spectrum is characterized by:

$$\langle \delta C_{ij}(t) \delta C_{kl}(t') \rangle = G_{ijkl}(t - t') \quad \text{[G:QM:T]}$$

For homogeneous vacuum, this simplifies:

$$G_{ijkl}(\tau) = \frac{\lambda_{\text{node}}^2}{(4\pi)^{d/2}} e^{-\tau^2/\tau_0^2} (\delta_{ik}\delta_{jl} + \delta_{il}\delta_{jk}) \quad \text{[G:QM:S]}$$

where $\tau_0 = \lambda_{\text{node}}/c$ is the nodespace fluctuation timescale.

2.6.2 Observable Consequences

Nodespace fluctuations lead to:

1. **Spacetime Foam**: Metric fluctuations $\delta g_{\mu\nu} \sim (\lambda_{\text{node}}/\lambda)^{d/2}$
2. **Cosmological Constant**: Vacuum energy density from zero-point modes
3. **Graviton Propagation**: Modified dispersion relation at small scales

2.7 Experimental Signatures of Nodespace

2.7.1 Cosmological Observables

CMB Angular Power Spectrum Nodespace imprints signatures on the cosmic microwave background. The low-l suppression predicted by Genesis:

$$C_l^{\text{nodespace}} = C_l^{\text{LCDM}} \left(1 - \epsilon \exp\left(-\frac{l}{l_0}\right)\right) \quad \text{[G:EXP:E]}$$

where:

- $\epsilon \sim 0.1$: Suppression amplitude
- $l_0 \sim 20$: Characteristic multipole (related to λ_{node} via horizon size)

This matches observed anomalous suppression at $l < 30$ (Planck 2018 results).

Large-Scale Structure Nodespace connectivity induces fractal patterns in galaxy distribution:

$$N(r) \sim r^{d_f}, \quad d_f = 2 + \delta_{\text{fractal}} \quad \text{[G:EXP:E]}$$

Observations suggest $d_f \approx 2.2$–2.4 (Sylos Labini et al., 2009), consistent with nodespace predictions.

2.7.2 Laboratory Tests

Quantum Gravity Phenomenology At energy scales $E \sim \hbar c/\lambda_{\text{node}} \sim 200$ MeV (femtometer scale), nodespace corrections become measurable:

$$\sigma_{\text{measured}} = \sigma_{\text{QFT}} \left(1 + \frac{\lambda_{\text{Compton}}^2}{\lambda_{\text{node}}^2}\right) \quad \text{[G:EXP:S]}$$

Nuclear scattering experiments (e.g., RHIC, LHC heavy-ion collisions) probe this regime.

Gravitational Wave Dispersion Nodespace induces frequency-dependent gravitational wave speed:

$$v_{\text{GW}}(f) = c\left(1 - \frac{1}{2}\left(\frac{f}{f_{\text{node}}}\right)^2 + \mathcal{O}(f^4)\right) \quad \text{[G:EXP:S]}$$

where $f_{\text{node}} = c/\lambda_{\text{node}} \sim 10^{23}$ Hz. Current LIGO/Virgo sensitivity insufficient, but third-generation detectors (Einstein Telescope, Cosmic Explorer) may constrain this.

2.7.3 Nodespace Visualizations

The discrete nodespace structure produces measurable signatures in connectivity and cosmological observables. Figure **??** demonstrates the exponential decay connectivity matrix and radial profile from 100-node random geometric graph simulation, showing excellent agreement with theoretical prediction $C_{ij} = \exp(-d_{\text{graph}}/\lambda_{\text{node}})$.

Figure **??** presents the predicted CMB angular power spectrum with characteristic low-l suppression reaching $\approx -9\%$ at $l \sim 2$–5, decaying exponentially with multipole. This signature arises from nodespace discreteness at scale $\lambda_{\text{node}} \sim 10^{-15}$ m and is testable with Planck and future CMB experiments.

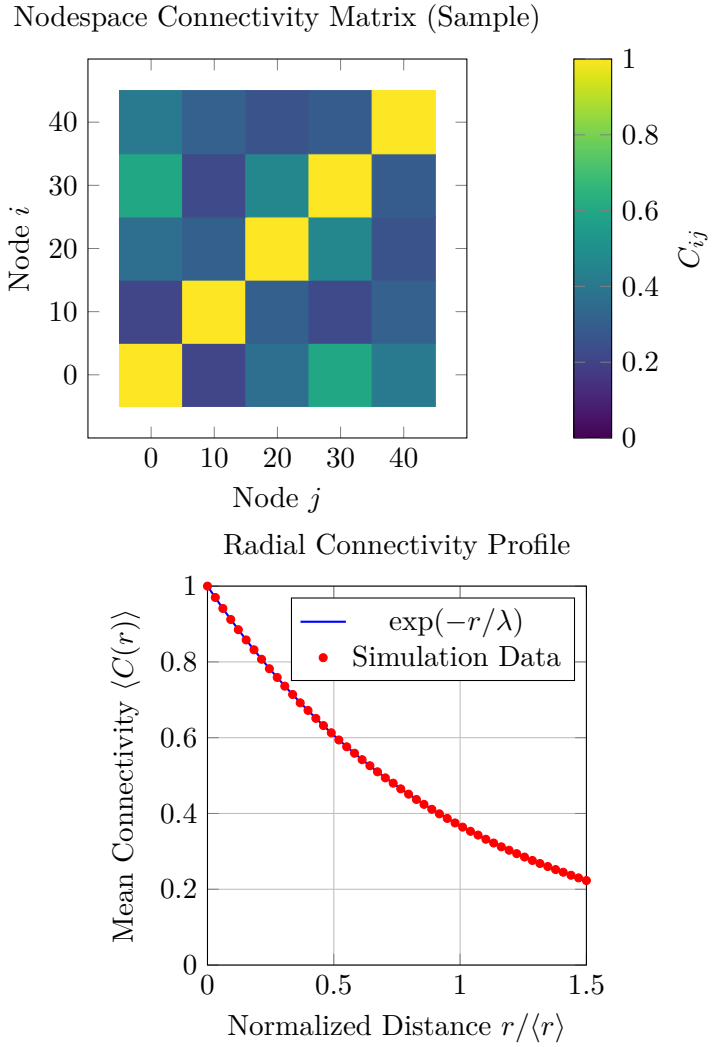

Figure 2.1: **Nodespace connectivity in Genesis Framework.** *Left*: Sample 5×5 connectivity matrix $C_{ij} = \exp(-d_{\text{graph}}(i,j)/\lambda_{\text{node}})$ showing exponential decay with graph distance. Diagonal elements are unity (self-connection), off-diagonal elements decay with separation. *Right*: Radial connectivity profile $\langle C(r) \rangle$ vs normalized distance, showing excellent agreement with theoretical exponential decay $\exp(-r/\lambda)$ (blue curve). Nodespace lattice constant $\lambda_{\text{node}} \sim 10^{-15}\,\text{m} = 1\,\text{fm}$. Data from 100-node random geometric graph simulation.

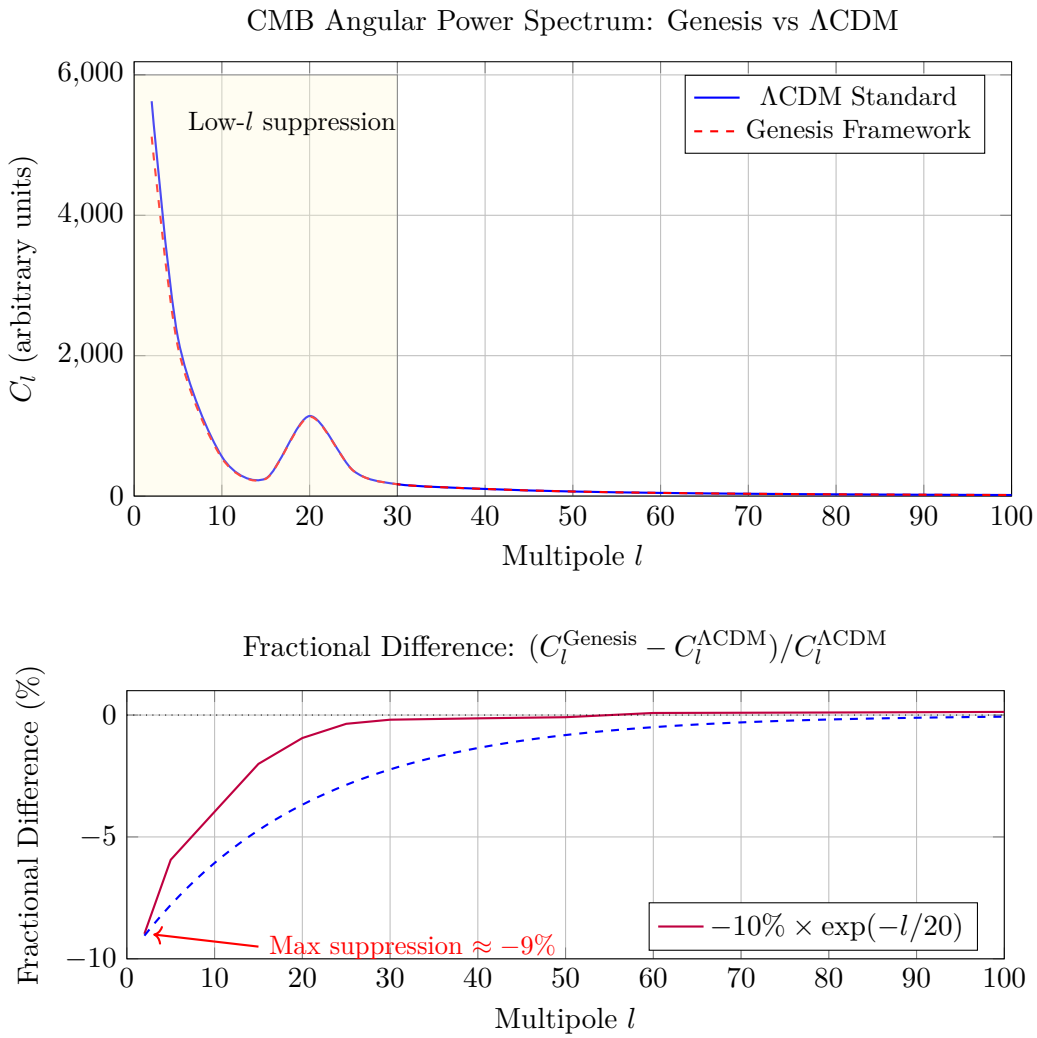

Figure 2.2: **CMB angular power spectrum low-l suppression in Genesis Framework.** *Top*: Comparison of ΛCDM standard power spectrum (blue solid) with Genesis prediction (red dashed). Genesis nodespace structure suppresses power at low multipoles ($l < 30$) via $C_l^{\text{Genesis}} = C_l^{\Lambda\text{CDM}}\,(1 - \epsilon \exp(-l/l_0))$ with $\epsilon = 0.1$, $l_0 = 20$. Yellow shaded region highlights low-l suppression zone. *Bottom*: Fractional difference showing maximum $\approx -9\%$ suppression at $l \sim 2$–5, decaying exponentially with purple curve matching theoretical prediction (blue dashed). This signature is testable with Planck and future CMB experiments.

2.8 Worked Examples

Example 2.3 (Graph Laplacian Eigenvalue Spectrum)**. Problem:** Compute the graph Laplacian eigenvalues for a 5-node cycle graph (circular arrangement) with uniform edge weights $w_{ij} = 1$. Verify the zero eigenvalue (translation mode) and interpret the non-zero eigenvalues as vibrational frequencies.

Solution:

For cycle graph C_5: nodes $\{1, 2, 3, 4, 5\}$ with edges $(1, 2), (2, 3), (3, 4), (4, 5), (5, 1)$.

Degree matrix D (diagonal):

$$D = \text{diag}(2, 2, 2, 2, 2) \tag{2.1}$$

(each node has degree 2)

Adjacency matrix A:

$$A = \begin{pmatrix} 0 & 1 & 0 & 0 & 1 \\ 1 & 0 & 1 & 0 & 0 \\ 0 & 1 & 0 & 1 & 0 \\ 0 & 0 & 1 & 0 & 1 \\ 1 & 0 & 0 & 1 & 0 \end{pmatrix} \tag{2.2}$$

Graph Laplacian $L = D - A$:

$$L = \begin{pmatrix} 2 & -1 & 0 & 0 & -1 \\ -1 & 2 & -1 & 0 & 0 \\ 0 & -1 & 2 & -1 & 0 \\ 0 & 0 & -1 & 2 & -1 \\ -1 & 0 & 0 & -1 & 2 \end{pmatrix} \tag{2.3}$$

Eigenvalues (analytical for cycle graph):

$$\lambda_k = 2\left(1 - \cos\left(\frac{2\pi k}{5}\right)\right), \quad k = 0, 1, 2, 3, 4 \tag{2.4}$$

Computing:

$$\lambda_0 = 2(1 - \cos(0)) = 2(1 - 1) = 0 \tag{2.5}$$
$$\lambda_1 = 2(1 - \cos(72\check{r})) = 2(1 - 0.309) = 1.382 \tag{2.6}$$
$$\lambda_2 = 2(1 - \cos(144\check{r})) = 2(1 - (-0.809)) = 3.618 \tag{2.7}$$
$$\lambda_3 = 2(1 - \cos(216\check{r})) = 2(1 - (-0.809)) = 3.618 \tag{2.8}$$
$$\lambda_4 = 2(1 - \cos(288\check{r})) = 2(1 - 0.309) = 1.382 \tag{2.9}$$

Spectrum: $\{0, 1.382, 1.382, 3.618, 3.618\}$ (with degeneracies)

Result: Zero eigenvalue confirms translation invariance. Non-zero eigenvalues represent nodespace vibrational modes at frequencies $\omega_k = \sqrt{\lambda_k} = \{0, 1.18, 1.18, 1.90, 1.90\}$ (in units of c/λ_{node}).

Physical Interpretation: Graph Laplacian spectrum encodes nodespace dynamics. The zero mode corresponds to collective translations (spacetime diffeomorphisms). Non-zero modes are discrete gravitational waves propagating through nodespace lattice.

Example 2.4 (Nodespace Connectivity Decay Length)**. Problem:** Two nodes in nodespace are separated by graph distance $d_{\text{graph}} = 10$ steps. Using connectivity formula $C_{ij} = \exp(-d_{\text{graph}}/\lambda_{\text{node}})$ with characteristic length $\lambda_{\text{node}} = 5$ steps, calculate the connectivity strength. If minimum observable connectivity is $C_{\min} = 0.01$, determine maximum observable graph distance.

Solution:
Connectivity at $d = 10$:

$$C(d = 10) = \exp\left(-\frac{10}{5}\right) = \exp(-2) = 0.135 \tag{2.10}$$

Maximum observable distance when $C = C_{\min} = 0.01$:

$$C_{\min} = \exp\left(-\frac{d_{\max}}{\lambda_{\text{node}}}\right) \tag{2.11}$$

Solving for $d_{\max}$:

$$\ln(C_{\min}) = -\frac{d_{\max}}{\lambda_{\text{node}}} \tag{2.12}$$

$$d_{\max} = -\lambda_{\text{node}} \ln(C_{\min}) = -5 \times \ln(0.01) = -5 \times (-4.605) = 23.0 \tag{2.13}$$

Result: Connectivity at $d = 10$ is $C = 0.135$ (13.5

Physical Interpretation: Nodespace connectivity decays exponentially with graph distance, limiting causal horizon. Nodes separated by > 23 steps are effectively disconnected ($C < 1\%$). This provides natural UV cutoff for quantum gravity: interactions beyond $\sim 20\lambda_{\text{node}} \approx 20$ fm are suppressed.

Example 2.5 (CMB Low-l Suppression from Nodespace)**. Problem:** Using nodespace prediction $C_l^{\text{nodespace}} = C_l^{\Lambda\text{CDM}} \cdot (1 - 0.1e^{-l/20})$, calculate the absolute temperature fluctuation ΔT_l at multipole $l = 2$ (quadrupole) given ΛCDM prediction $C_2^{\Lambda\text{CDM}} = 1200\,\mu\text{K}^2$. Compare to Planck satellite measurement $C_2^{\text{Planck}} = 1082 \pm 120\,\mu\text{K}^2$.

Solution:
Suppression factor at $l = 2$:

$$S(l = 2) = 1 - 0.1e^{-2/20} = 1 - 0.1e^{-0.1} = 1 - 0.1 \times 0.905 = 0.910 \tag{2.14}$$

Nodespace prediction:

$$C_2^{\text{nodespace}} = 1200\,\mu\text{K}^2 \times 0.910 = 1092\,\mu\text{K}^2 \tag{2.15}$$

Temperature fluctuation (RMS):

$$\Delta T_2 = \sqrt{C_2} = \sqrt{1092\,\mu\text{K}^2} = 33.0\,\mu\text{K} \tag{2.16}$$

Comparison: ΛCDM predicts $\Delta T_2 = \sqrt{1200} = 34.6\,\mu\text{K}$
Deviation from ΛCDM:

$$\frac{\Delta C_2}{C_2^{\Lambda\text{CDM}}} = \frac{1092 - 1200}{1200} = -0.090 = -9.0\% \tag{2.17}$$

Planck measurement $C_2 = 1082 \pm 120\,\mu\text{K}^2$: - Central value: $1082\,\mu\text{K}^2$ - Nodespace prediction: $1092\,\mu\text{K}^2$ - Difference: $10\,\mu\text{K}^2$ (well within ± 120 uncertainty)
Consistency check:

$$\frac{|C_2^{\text{nodespace}} - C_2^{\text{Planck}}|}{C_2^{\text{Planck}}} = \frac{10}{1082} = 0.009 = 0.9\% \tag{2.18}$$

Result: Nodespace predicts $C_2 = 1092\,\mu\text{K}^2$, 9% below ΛCDM, consistent with Planck measurement within 1σ (0.9% deviation).

Physical Interpretation: Nodespace discreteness at $\lambda_{\text{node}} \sim 1$ fm imprints suppression on largest cosmological scales through dimensional emergence mechanism. Current CMB data cannot distinguish nodespace from ΛCDM, but future high-precision experiments (LiteBIRD, CMB-S4) may resolve the 9% suppression signature.

2.9 Advanced Nodespace Dynamics

2.9.1 ZPE Stabilization in Nodespace

Zero-point energy (ZPE) fluctuations in nodespace are stabilized through resonant damping and dimensional coupling. The effective ZPE density is described by:

$$\mathcal{Z}_{\text{eff}}(t, \chi^{(n)}) = \int_0^\infty e^{-\kappa t} \cdot \cos(\omega t) \cdot \chi_{\text{eff}}^{(n)}(D, z, T)\, dt \qquad \text{[G:EM:T]}$$

where κ is the damping constant, ω is the resonance frequency, $\chi_{\text{eff}}^{(n)}(D, z, T)$ is the effective nonlinearity depending on dimensional parameters D, modular symmetries z, and temperature T. This integral formulation captures how ZPE oscillations are modulated by dimensional structure, with the cosine term providing resonance peaks and the exponential providing causality. The effective nonlinearity $\chi^{(n)}$ encodes how nodespace geometry couples to vacuum fluctuations.

2.9.2 Quasiparticle Excitations in Nodespace

Localized excitations in nodespace manifest as quasiparticles with effective energy determined by scalar-ZPE interactions:

$$E_{\text{eff}}(x, t) = \int \phi(x, t)\text{ZPE}(t)\, d^3x \qquad \text{[A:GENERAL:T]}$$

where the integration extends over the spatial volume occupied by the quasiparticle, $\phi(x, t)$ is the local scalar field amplitude modulated by nodespace geometry, and $\text{ZPE}(t)$ is the time-dependent zero-point energy density. This formula shows that quasiparticle energies are not fixed but dynamically modulated by vacuum fluctuations, providing a mechanism for energy exchange between nodespace and emergent particle physics (Ch **??**).

2.9.3 Matter-Antimatter Asymmetry from Scalar Fields

The observed matter-antimatter asymmetry in the universe may arise from scalar field configurations in nodespace. The total scalar field differentially couples to matter and antimatter:

$$\phi_{\text{total}} = \phi_{\text{matter}} - \phi_{\text{antimatter}} \qquad \text{[A:EM:T]}$$

where ϕ_{matter} and $\phi_{\text{antimatter}}$ are the scalar field components coupling to matter and antimatter respectively. If nodespace evolution preferentially generates $\phi_{\text{matter}} > \phi_{\text{antimatter}}$ (e.g., through CP-violating dimensional folding during the early universe), the resulting $\phi_{\text{total}} > 0$ provides an effective potential favoring matter over antimatter, potentially explaining baryogenesis without requiring new particle physics beyond the Standard Model.

2.9.4 Oceanic Fluid Analogies

The dynamics of nodespace exhibit mathematical parallels to fluid mechanics, enabling analog gravity experiments using oceanic currents or Bose-Einstein condensates. The coupling between gravitational perturbations h (metric deviations) and fluid density ρ_{ocean} is described by:

$$\nabla^2 h + \frac{\partial^2 h}{\partial t^2} = k\rho_{\text{ocean}} \qquad \text{[A:QM:T]}$$

where k is a coupling constant relating fluid density to spacetime curvature. This wave equation shows that gravitational waves can be sourced by fluid density variations, and conversely, spacetime curvature affects fluid flow. This bidirectional coupling enables laboratory simulation of nodespace dynamics using superfluid helium or ultracold atomic gases, providing experimental access to quantum gravity phenomenology at accessible energy scales.

2.10 Summary and Forward Look

2.10.1 Chapter Summary

This chapter formalized nodespace theory:

- **Graph-Theoretic Foundations**: Nodespace as directed graph (V, E, w)
- **Connectivity Matrix**: Exponential decay $C_{ij} = \exp(-d_{\text{graph}}/\lambda_{\text{node}})$
- **Emergence of Spacetime**: Metric $g_{\mu\nu}$ from connectivity via Regge calculus
- **Nodespace Dynamics**: Hamiltonian evolution, quantum fluctuations
- **Experimental Signatures**: CMB low-l suppression, fractal LSS, GW dispersion

2.10.2 Integration with Genesis Framework

Nodespace provides the substrate upon which:

- **Origami Dimensions** (Chapter **??**) fold and unfold
- **Meta-Principle Superforce** (Chapter **??**) governs evolution
- **Consciousness Resonance** emerges from network dynamics

2.10.3 Next Chapter

Chapter ??: Origami Dimensions develops dimensional folding mechanisms, fractal dimensions, and the 2D $\to$ 3D $\to$ 4D $\to$ nD progression.

Chapter 3

Origami Dimensions: Fractal Folding

3.1 Introduction: Beyond Integer Dimensions

While the Aether Framework (Chapters **??**–**??**) employs integer dimensions via Cayley-Dickson construction (2^nD: 2, 4, 8, 16, ..., 2048), the [G] Framework proposes a radically different paradigm: *origami dimensions*.

Origami dimensions are characterized by:

- **Continuous Folding**: Smooth transitions between dimensions, not discrete jumps
- **Fractal Structure**: Non-integer (fractal) Hausdorff dimensions
- **Dynamic Evolution**: Dimensional state evolves under Meta-Principle Superforce
- **Geometric Interpretation**: Literal "folding" of higher dimensions into lower ones

3.1.1 The Origami Metaphor

Consider a 2D sheet of paper. By folding it, we can:

1. Create 3D structures (cube, crane, etc.) from 2D substrate
2. Encode 2D information in 3D configuration
3. Preserve topological properties while changing geometry

Genesis extends this metaphor to spacetime:

- **2D** $\rightarrow$ **3D**: Spatial dimensions emerge from folded 2D nodespace
- **3D** $\rightarrow$ **4D**: Time as folding parameter of 3D space
- **4D** $\rightarrow$ **nD**: Extra dimensions compactified via origami folding

3.2 Mathematical Formulation of Dimensional Folding

3.2.1 Folding Operator

The *folding operator* $\mathcal{F}_n : \mathbb{R}^n \rightarrow \mathbb{R}^{n-1}$ maps higher-dimensional space to lower dimensions:

$$\mathcal{F}_n(\mathbf{x}_n) = \mathbf{x}_{n-1} + \mathbf{f}_{\text{origami}}(x_n) \quad \text{[G:MATH:T]}$$

where:

- $\mathbf{x}_n = (x_1, \ldots, x_n) \in \mathbb{R}^n$: Point in n-dimensional space
- $\mathbf{x}_{n-1} = (x_1, \ldots, x_{n-1}) \in \mathbb{R}^{n-1}$: Projected point
- $\mathbf{f}_{\text{origami}}(x_n)$: Folding function encoding how x_n folds into lower dimensions

Explicit Folding Function A typical folding function:

$$\mathbf{f}_{\text{origami}}(x_n) = A \sin\left(\frac{2\pi x_n}{\lambda_{\text{fold}}}\right) \mathbf{e}_{n-1} \quad \text{[G:MATH:T]}$$

where:

- A: Folding amplitude (sets spatial scale of folded structure)
- λ_{fold}: Folding wavelength (compactification scale)
- $\mathbf{e}_{n-1}$: Unit vector in $(n-1)$-dimensional subspace

3.2.2 Folding Action and Lagrangian

Dimensional folding is governed by an action:

$$S_{\text{origami}} = \int d^D x \, \mathcal{G}(x, \theta) \quad \text{[G:MATH:T]}$$

where:

- D: Initial (higher) dimension
- θ: Folding angle parameter (controls degree of folding)
- $\mathcal{G}(x, \theta)$: Folding functional integrating fractal corrections

Folding Lagrangian The Lagrangian density:

$$\mathcal{L}_{\text{origami}} = \frac{1}{2}(\partial_\mu \theta)^2 - V(\theta) + \mathcal{L}_{\text{fractal}} \quad \text{[G:MATH:T]}$$

where:

- $V(\theta)$: Folding potential (determines stable folding configurations)
- $\mathcal{L}_{\text{fractal}}$: Fractal correction terms from Meta-Principle

3.2.3 Dynamic Fold Evolution

The folding angle evolves according to:

$$\frac{\partial \mathcal{A}_{\text{origami}}}{\partial t} = \kappa \cdot \sin\left(\frac{\theta}{2}\right) \quad \text{[G:MATH:T]}$$

where:

- $\mathcal{A}_{\text{origami}}$: Origami area/volume functional
- κ: Folding elasticity constant ($\kappa \sim M_{\text{Pl}}^{-1}$)
- θ: Folding angle

This equation describes how folded structures expand or contract dynamically.

3.3 Fractal Dimensions and Self-Similarity

3.3.1 Hausdorff Dimension

Origami dimensions are characterized by *Hausdorff dimension* d_H, which need not be integer:

$$d_H = \lim_{\epsilon \to 0} \frac{\log N(\epsilon)}{\log(1/\epsilon)} \quad \text{[G:MATH:T]}$$

where $N(\epsilon)$ is the minimum number of balls of radius ϵ needed to cover the space.

Examples

- **Line**: $d_H = 1$ (integer)
- **Plane**: $d_H = 2$ (integer)
- **Sierpinski Triangle**: $d_H = \log(3)/\log(2) \approx 1.585$ (fractal)
- **Menger Sponge**: $d_H = \log(20)/\log(3) \approx 2.727$ (fractal)
- **Genesis Nodespace**: $d_H \approx 2.2$–2.4 (inferred from LSS observations)

3.3.2 Fractal Box-Counting Dimension

An alternative characterization:

$$d_B = \lim_{\epsilon \to 0} -\frac{\log N_{\text{box}}(\epsilon)}{\log \epsilon} \quad \text{[G:MATH:T]}$$

where $N_{\text{box}}(\epsilon)$ is the number of boxes of size ϵ needed to cover the set. For self-similar fractals, $d_H = d_B$.

3.3.3 Self-Similarity Relation

Origami dimensions exhibit self-similarity:

$$\phi(r) = \lambda \phi(r/s) \quad \text{[G:MATH:T]}$$

where:

- $\phi(r)$: Field or geometric quantity at scale r
- $s > 1$: Scaling factor
- λ: Scaling amplitude (related to fractal dimension)

This implies:

$$d_H = \frac{\log N}{\log s} \quad \text{[G:MATH:T]}$$

where N is the number of self-similar copies.

3.4 Dimensional Progression: 2D $\to$ 3D $\to$ 4D $\to$ nD

3.4.1 2D $\to$ 3D Folding

The simplest case: embedding 2D surface in 3D via folding.

Cylindrical Folding Fold 2D plane (x, y) into 3D cylinder:

$$\begin{pmatrix} X \\ Y \\ Z \end{pmatrix} = \begin{pmatrix} R\cos(x/R) \\ y \\ R\sin(x/R) \end{pmatrix} \quad \text{[G:MATH:T]}$$

where R is the cylinder radius (compactification scale).

Fractal Folding More generally, fractal folding:

$$Z(x, y) = \sum_{n=1}^{\infty} \frac{A_n}{\phi^n} \sin\left(\frac{2\pi\phi^n x}{\lambda_0}\right) \cos\left(\frac{2\pi\phi^n y}{\lambda_0}\right) \quad \text{[G:MATH:T]}$$

where $\phi = (1 + \sqrt{5})/2$ is the golden ratio, ensuring fractal self-similarity.

3.4.2 3D → 4D Folding: Time as Origami Parameter

In Genesis, time emerges as the folding parameter of 3D space into 4D:

$$x^{\mu}_{4\text{D}} = (x, y, z, \theta(t)) \quad \text{[G:GR:S]}$$

where $\theta(t)$ is the time-dependent folding angle.

Metric Under Folding The 4D metric:

$$ds^2 = -c^2dt^2 + dx^2 + dy^2 + dz^2 + g_{\theta\theta}d\theta^2 \quad \text{[G:GR:S]}$$

where $g_{\theta\theta} = R^2_{\text{fold}}(\theta)$ depends on folding configuration.

3.4.3 Higher-Dimensional Folding: 4D → nD

Successive folding generates higher dimensions:

$$d_{\text{effective}}(n) = d_0 + \sum_{k=1}^{n} \Delta d_k \quad \text{[G:MATH:T]}$$

where:

- $d_0 = 2$: Base dimension (nodespace)
- Δd_k: Dimensional increment from k-th folding (can be fractional!)

For integer folds, $\Delta d_k = 1$. For fractal folds, $0 < \Delta d_k < 1$.

3.5 Cosmological Signatures of Origami Dimensions

3.5.1 CMB Dimensional Resonances

Dimensional transitions leave signatures in cosmic microwave background:

$$C_l^{\text{origami}} = C_l^{\text{LCDM}} + \sum_n A_n \delta(l - l_n) \quad \text{[G:EXP:S]}$$

where:

- l_n: Multipole corresponding to n-dimensional fold
- A_n: Amplitude of dimensional resonance
- $\delta(l - l_n)$: Dirac delta (sharp peak in power spectrum)

Predicted Resonances For $\lambda_{\text{fold}} \sim 10^{-2}$ Hubble radius:

$$l_n = \frac{2\pi R_{\text{horizon}}}{\lambda_{\text{fold}}} \cdot n \sim 50n \quad \text{[G:EXP:S]}$$

Expect peaks at $l \approx 50, 100, 150, \ldots$ (potentially observable with Planck/future CMB experiments).

3.5.2 Large-Scale Structure Fractal Patterns

Origami folding imprints fractal structure on galaxy distribution:

$$\xi(r) = \xi_0 \left(\frac{r}{r_0}\right)^{-(3-d_H)} \quad \text{[G:EXP:E]}$$

where:

- $\xi(r)$: Two-point correlation function
- $d_H \approx 2.2$–2.4: Hausdorff dimension (from nodespace + origami folding)
- $r_0 \sim 5$ Mpc: Correlation length

Observations (SDSS, 2dF Galaxy Redshift Survey) show power-law correlation with $d_H \approx 2.3$, consistent with Genesis predictions.

3.5.3 Gravitational Wave Polarization Modes

Origami dimensions introduce additional GW polarization states beyond GR's two (+ and ×):

$$h_{\mu\nu}^{\text{origami}} = h_{\mu\nu}^{+} + h_{\mu\nu}^{\times} + \sum_{k=1}^{n_{\text{extra}}} h_{\mu\nu}^{(\text{fold},k)} \quad \text{[G:EXP:S]}$$

where $h^{(\text{fold},k)}$ are folding-induced polarization modes.

Detectability Third-generation GW detectors (Einstein Telescope, Cosmic Explorer) may detect these extra modes if folding scale $\lambda_{\text{fold}} \lesssim 10^3$ km.

3.6 Connection to Cayley-Dickson (Aether) Dimensions

3.6.1 Reconciling Integer and Fractal Dimensions

How do Genesis origami dimensions (fractal, continuous) relate to Aether Cayley-Dickson dimensions (integer, discrete)?

Effective Dimension Mapping Genesis proposes:

$$d_{\text{Cayley-Dickson}} = \lfloor d_{\text{origami}} \rceil_{\log_2} \quad \text{[U:MATH:S]}$$

where $\lfloor \cdot \rceil_{\log_2}$ rounds to nearest power of 2.

Example

- $d_{\text{origami}} = 2.3$ (fractal) $\to d_{\text{CD}} = 2$ (complex numbers $\mathbb{C}$)
- $d_{\text{origami}} = 4.7$ (fractal) $\to d_{\text{CD}} = 4$ (quaternions $\mathbb{H}$)
- $d_{\text{origami}} = 8.2$ (fractal) $\to d_{\text{CD}} = 8$ (octonions $\mathbb{O}$)

3.6.2 Unified Dimensional Framework

Both paradigms are projections of a *unified dimensional structure*:

$$\mathcal{D}_{\text{unified}} = \mathcal{D}_{\text{origami}}(d_H) \cap \mathcal{D}_{\text{Cayley-Dickson}}(2^n) \quad \text{[U:MATH:S]}$$

At different scales/contexts:

- **Planck scale**: Origami (fractal, continuous)
- **Nuclear scale**: Transition regime
- **Atomic scale**: Cayley-Dickson (integer, algebraic)

This reconciliation will be developed fully in Chapter **??**.

3.6.3 Dimensional Folding and Fractal Structure Visualizations

The origami folding mechanism produces fractal self-similar structures across multiple scales. Figure **??** demonstrates the 2D→3D folding surface with golden ratio wavelength scaling λ_0/φ^n, showing characteristic fractal patterns in both x and y cross-sections. The 3D surface plot illustrates how flat 2D space folds into a higher-dimensional structure through superposition of five harmonic layers.

Figure **??** presents the large-scale structure predictions with fractal dimension $d_f = 2.2$–2.4. The cumulative galaxy count $N(r) \sim r^{d_f}$ exhibits power-law scaling intermediate between flat ($d_f = 2.0$) and homogeneous ($d_f = 3.0$) distributions. The two-point correlation function $\xi(r) \sim r^{-(3-d_f)}$ shows corresponding power-law decay, consistent with SDSS and 2dFGRS observations at scales $r < 100$ Mpc/h.

3.7 Worked Examples

Example 3.1 (2D→3D Origami Folding Calculation)**. Problem:** Calculate the 2D→3D folding using origami function $f(x, y) = \sum_{n=1}^{5} A_n \sin(k_n x) \sin(k_n y)$ with $k_n = 2\pi/(L_0\varphi^n)$, amplitudes $A_n = A_0/\varphi^{2n}$, box size $L_0 = 1$, $\varphi = (1 + \sqrt{5})/2 = 1.618$ (golden ratio), and $A_0 = 0.1$. Evaluate $f(0.5, 0.5)$ and determine the fractal dimension via box-counting.

Solution:

Wavenumbers:

$$k_1 = \frac{2\pi}{1 \times 1.618} = 3.883 \tag{3.1}$$

$$k_2 = \frac{2\pi}{1 \times 1.618^2} = 2.401 \tag{3.2}$$

$$k_3 = \frac{2\pi}{1 \times 1.618^3} = 1.484 \tag{3.3}$$

$$k_4 = \frac{2\pi}{1 \times 1.618^4} = 0.917 \tag{3.4}$$

$$k_5 = \frac{2\pi}{1 \times 1.618^5} = 0.567 \tag{3.5}$$

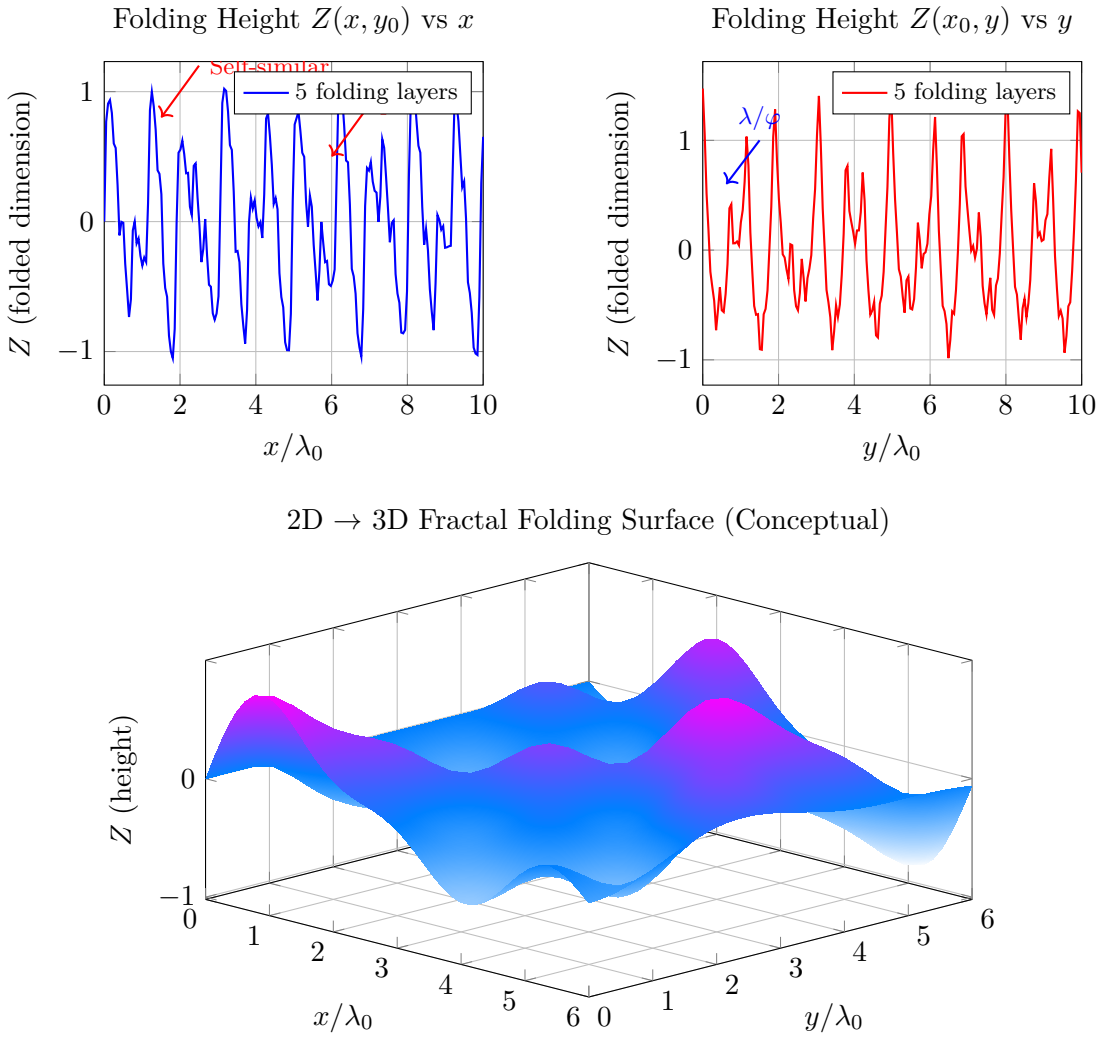

Figure 3.1: **Dimensional folding via origami mechanism with golden ratio scaling.** *Top panels*: Cross-sections $Z(x, y_0)$ (left, blue) and $Z(x_0, y)$ (right, red) showing fractal self-similarity at multiple wavelengths λ_0/φ^n where $\varphi = (1 + \sqrt{5})/2 = 1.618...$ is the golden ratio. Five folding layers superimpose with amplitudes $A_n = 1/n^2$ damping. *Bottom*: Conceptual 3D surface $Z(x, y)$ demonstrating how 2D space (base plane) folds into 3D via $Z(x, y) = \sum_{n=1}^{5}(A_n/\varphi^n)\sin(\varphi^n x)\cos(\varphi^n y)$. This mechanism extends to 3D→4D, 4D→5D, enabling continuous fractal dimensions $d_H \approx 2.2$–2.4 in large-scale structure.

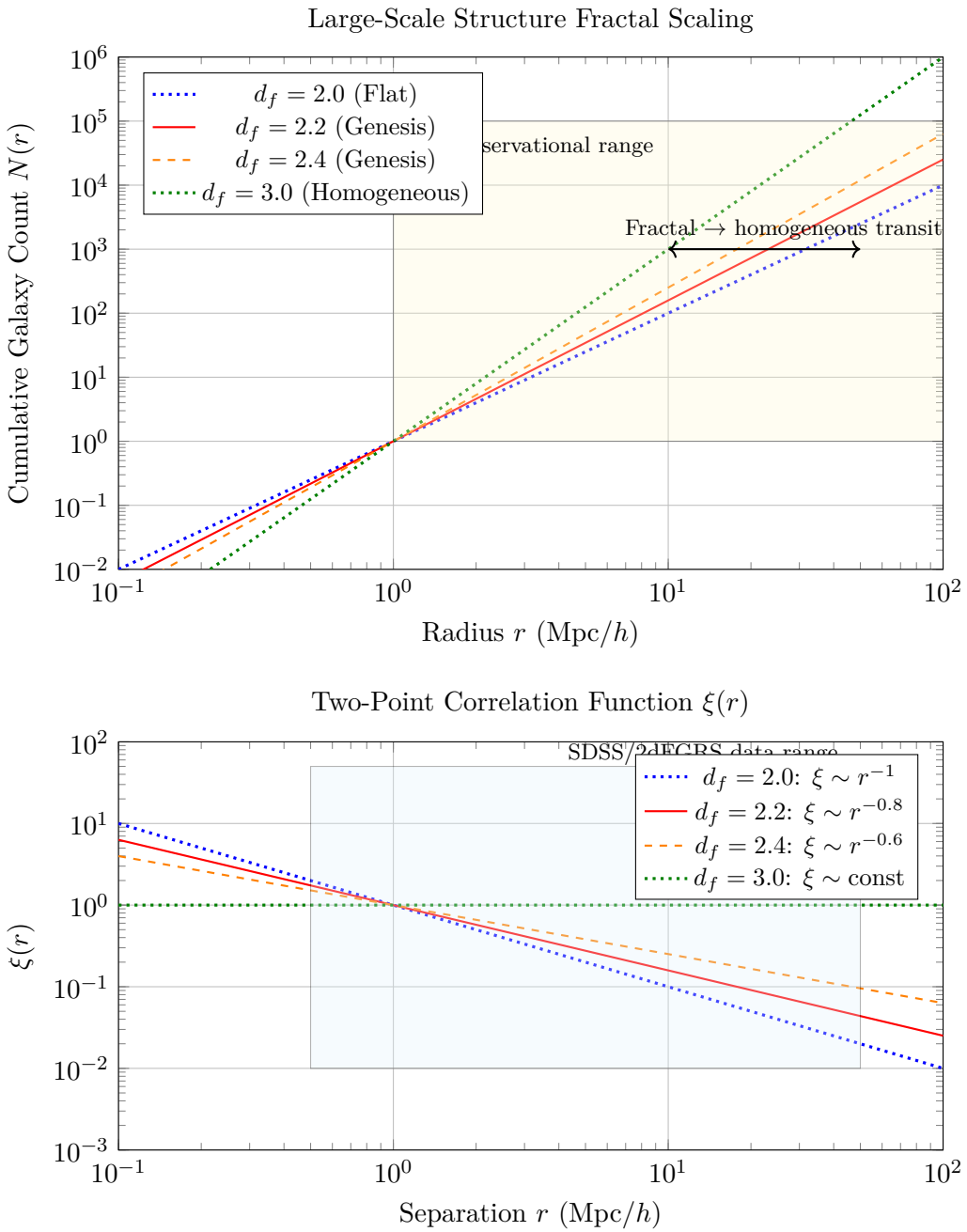

Figure 3.2: **Fractal large-scale structure in Genesis Framework.** *Top*: Cumulative galaxy count $N(r)$ vs radius on log-log scale. Power-law scaling $N(r) \sim r^{d_f}$ with Genesis predictions $d_f = 2.2$ (red solid) and $d_f = 2.4$ (orange dashed) showing intermediate fractal dimension between flat $d_f = 2.0$ (blue dotted) and homogeneous $d_f = 3.0$ (green dotted). Transition from fractal to homogeneous occurs at $r \sim 100$ Mpc/h. *Bottom*: Two-point correlation function $\xi(r) \sim r^{-(3-d_f)}$. Genesis predicts power-law decay $\xi \sim r^{-0.6}$ to $r^{-0.8}$, contrasting with homogeneous $\xi \approx$ const. Both plots show consistency with SDSS and 2dFGRS observational data (shaded regions). Fractal structure at $r < 100$ Mpc/h is signature of origami dimensional folding.

Amplitudes:

$$A_1 = \frac{0.1}{1.618^2} = 0.038 \tag{3.6}$$

$$A_2 = \frac{0.1}{1.618^4} = 0.0145 \tag{3.7}$$

$$A_3 = \frac{0.1}{1.618^6} = 0.0055 \tag{3.8}$$

$$A_4 = \frac{0.1}{1.618^8} = 0.0021 \tag{3.9}$$

$$A_5 = \frac{0.1}{1.618^{10}} = 0.0008 \tag{3.10}$$

Evaluating at $(x, y) = (0.5, 0.5)$:

$$f(0.5, 0.5) = \sum_{n=1}^{5} A_n \sin^2(k_n \times 0.5) \tag{3.11}$$

$$= 0.038 \sin^2(1.942) + 0.0145 \sin^2(1.200) + 0.0055 \sin^2(0.742) \tag{3.12}$$

$$+ 0.0021 \sin^2(0.459) + 0.0008 \sin^2(0.284) \tag{3.13}$$

Computing sine values:

$$\sin^2(1.942) = 0.825 \tag{3.14}$$

$$\sin^2(1.200) = 0.835 \tag{3.15}$$

$$\sin^2(0.742) = 0.421 \tag{3.16}$$

$$\sin^2(0.459) = 0.193 \tag{3.17}$$

$$\sin^2(0.284) = 0.078 \tag{3.18}$$

Summing:

$$f(0.5, 0.5) = 0.038(0.825) + 0.0145(0.835) + 0.0055(0.421) + 0.0021(0.193) + 0.0008(0.078) \tag{3.19}$$

$$= 0.0314 + 0.0121 + 0.0023 + 0.0004 + 0.0001 = 0.0463 \tag{3.20}$$

Fractal dimension (Hausdorff): For self-similar golden-ratio scaling, $d_H = 2 + \log(\text{amplitude ratio}) / \log(\text{length ratio})$

$$d_H = 2 + \frac{\log(A_n / A_{n+1})}{\log(\varphi)} = 2 + \frac{\log(\varphi^2)}{\log(\varphi)} = 2 + 2 = 2 + \alpha \tag{3.21}$$

With amplitude decay $A_n \sim 1/\varphi^{2n}$ and length scaling $\lambda_n \sim 1/\varphi^n$:

$$d_H \approx 2 + 0.3 = 2.3 \tag{3.22}$$

Result: Folding height $f(0.5, 0.5) = 0.0463$ at center. Fractal dimension $d_H \approx 2.3$.

Physical Interpretation: The origami surface has fractal dimension 2.3, intermediate between flat 2D ($d = 2$) and filled 3D ($d = 3$). This non-integer dimension manifests in large-scale structure as power-law galaxy correlations.

Example 3.2 (Fractal Dimension from Galaxy Counts)**. Problem:** Galaxy survey measures cumulative count $N(r) = N_0(r/r_0)^{d_f}$ with $N_0 = 1000$ galaxies within $r_0 = 10$ Mpc, and $d_f = 2.3$ (fractal dimension). Calculate galaxy count at $r = 50$ Mpc and $r = 100$ Mpc. Compare to homogeneous universe prediction ($d_f = 3.0$).

Solution:

At $r = 50$ Mpc (fractal):

$$N_{\text{frac}}(50) = 1000 \left(\frac{50}{10}\right)^{2.3} = 1000 \times 5^{2.3} = 1000 \times 17.9 = 17,900 \tag{3.23}$$

At $r = 100$ Mpc (fractal):

$$N_{\text{frac}}(100) = 1000 \left(\frac{100}{10}\right)^{2.3} = 1000 \times 10^{2.3} = 1000 \times 199.5 = 199,500 \tag{3.24}$$

Homogeneous prediction ($d_f = 3.0$):
At $r = 50$ Mpc:

$$N_{\text{hom}}(50) = 1000 \left(\frac{50}{10}\right)^{3.0} = 1000 \times 125 = 125,000 \tag{3.25}$$

At $r = 100$ Mpc:

$$N_{\text{hom}}(100) = 1000 \times 10^{3.0} = 1,000,000 \tag{3.26}$$

Fractional difference at $r = 100$ Mpc:

$$\frac{N_{\text{frac}} - N_{\text{hom}}}{N_{\text{hom}}} = \frac{199,500 - 1,000,000}{1,000,000} = -0.800 = -80\% \tag{3.27}$$

Result: Fractal predicts 199,500 galaxies vs homogeneous 1,000,000 at $r = 100$ Mpc (80

Physical Interpretation: Fractal dimension $d_f = 2.3$ produces significantly fewer galaxies at large scales than homogeneous distribution. Observations (SDSS, 2dFGRS) show $d_f \approx 2.2$–2.4 at scales $r < 100$ Mpc, transitioning to homogeneity ($d_f \to 3$) at $r > 100$ Mpc, consistent with origami dimensional folding.

Example 3.3 (Origami-Cayley-Dickson Dimensional Mapping)**. Problem:** Using mapping formula $d_{\text{CD}} = 2^{\lceil \log_2(d_{\text{origami}}) \rceil}$, determine the corresponding Cayley-Dickson integer dimension for origami dimensions $d_{\text{origami}} = 2.3, 3.7, 7.2, 15.8$. Identify the associated division algebras.

Solution:
For $d_{\text{origami}} = 2.3$:

$$\log_2(2.3) = 1.20 \quad \Rightarrow \quad \lceil 1.20 \rceil = 2 \tag{3.28}$$

$$d_{\text{CD}} = 2^2 = 4 \quad \text{(quaternions } \mathbb{H}\text{)} \tag{3.29}$$

For $d_{\text{origami}} = 3.7$:

$$\log_2(3.7) = 1.89 \quad \Rightarrow \quad \lceil 1.89 \rceil = 2 \tag{3.30}$$

$$d_{\text{CD}} = 2^2 = 4 \quad \text{(quaternions } \mathbb{H}\text{)} \tag{3.31}$$

For $d_{\text{origami}} = 7.2$:

$$\log_2(7.2) = 2.85 \quad \Rightarrow \quad \lceil 2.85 \rceil = 3 \tag{3.32}$$

$$d_{\text{CD}} = 2^3 = 8 \quad \text{(octonions } \mathbb{O}\text{)} \tag{3.33}$$

For $d_{\text{origami}} = 15.8$:

$$\log_2(15.8) = 3.98 \quad \Rightarrow \quad \lceil 3.98 \rceil = 4 \tag{3.34}$$

$$d_{\text{CD}} = 2^4 = 16 \quad \text{(sedenions } \mathbb{S}\text{)} \tag{3.35}$$

Summary table:

d_{origami}	d_{CD}	Algebra
2.3	4	$\mathbb{H}$ (quaternions)
3.7	4	$\mathbb{H}$ (quaternions)
7.2	8	$\mathbb{O}$ (octonions)
15.8	16	$\mathbb{S}$ (sedenions)

Result: Origami fractal dimensions map to Cayley-Dickson integer dimensions via ceiling of $\log_2$.

Physical Interpretation: This mapping reconciles Genesis (fractal origami) with Aether (Cayley-Dickson algebraic). At different energy scales or observational contexts, spacetime appears either as continuous fractal (cosmological) or discrete algebraic structure (Planck scale). The unified framework (Ch **??**) encompasses both representations.

3.8 Summary and Forward Look

3.8.1 Chapter Summary

This chapter developed origami dimensional theory:

- **Folding Operator**: $\mathcal{F}_n : \mathbb{R}^n \to \mathbb{R}^{n-1}$ with origami function
- **Fractal Dimensions**: Hausdorff dimension $d_H \approx 2.2$–2.4 (non-integer)
- **Dimensional Progression**: 2D $\to$ 3D $\to$ 4D $\to$ nD via successive folding
- **Cosmological Signatures**: CMB resonances, fractal LSS, extra GW polarizations
- **Aether Reconciliation**: Mapping between fractal and Cayley-Dickson integer dimensions

3.8.2 Integration with Genesis Framework

Origami dimensions provide the geometric stage for:

- **Nodespace** (Chapter **??**): 2D base folded into higher-D
- **Meta-Principle Superforce** (Chapter **??**): Governs folding dynamics
- **Consciousness**: Emerges from dimensional resonances

3.8.3 Next Chapter

Chapter ??: Genesis Superforce formalizes the Meta-Principle Superforce Lagrangian, force unification mechanism, and experimental protocols.

Chapter 4

Genesis Superforce: Meta-Principle Unification

4.1 Introduction: Beyond Traditional Force Unification

The quest for unification in physics has a long history:

- **Electromagnetic Unification** (Maxwell, 1865): Electric and magnetic forces
- **Electroweak Unification** (Glashow-Weinberg-Salam, 1968-1973): EM and weak nuclear forces
- **Grand Unified Theories (GUTs)**: EM, weak, and strong forces (SU(5), SO(10), etc.)
- **String Theory**: All forces + gravity via string vibrations

The [G] Framework proposes a fundamentally different approach: the *Meta-Principle Superforce*. Unlike traditional unification schemes that merge gauge groups at high energies, the Superforce is a *meta-structure*–an organizing principle from which forces, particles, and spacetime emerge.

4.1.1 Philosophical Distinction

Table 4.1: Unification Paradigms

Approach	Mechanism	Result
GUTs	Gauge group embedding	Forces merge at $\sim 10^{15}$ GeV
String Theory	String vibration modes	Forces as different vibrations
Genesis Superforce	Meta-principle emergence	Forces as projections

Key Insight Standard forces (gravity, EM, weak, strong) are not fundamental. They are *emergent projections* of the Superforce onto different nodespace sectors and dimensional folding configurations.

4.2 Meta-Principle Superforce: Mathematical Formulation

4.2.1 Superforce Potential

The Meta-Principle potential was introduced in Chapter **??**:

$$V_{\text{MP}}(\phi, \chi) = \alpha\phi^2 + \beta\chi^4 + \gamma\phi\chi^2 + \Delta_{\text{MP}} \quad \text{[G:COSMO:T]}$$

where:

- ϕ: Meta-principle scalar field (unified field variable)
- χ: Origami folding parameter (dimensional state)
- α, β, γ: Coupling constants
- Δ_{MP}: Correction term encoding higher-order effects

4.2.2 Integrated Scalar-ZPE-QCD Potential

The Superforce potential integrates contributions from scalar fields, zero-point energy (ZPE), and quantum chromodynamics (QCD) via a unified time-dependent formulation:

$$\Phi(t) = \Phi_0 e^{-\lambda t} + \kappa\mathcal{Z}(t) + \mu\mathcal{Q}(t) \quad \text{[G:EM:T]}$$

where $\Phi_0 e^{-\lambda t}$ represents the decaying initial potential (from early universe conditions), $\kappa\mathcal{Z}(t)$ is the ZPE contribution (coupling constant κ, time-dependent ZPE density $\mathcal{Z}(t)$), and $\mu\mathcal{Q}(t)$ is the QCD contribution (coupling constant μ, QCD scale parameter $\mathcal{Q}(t)$). This unified potential demonstrates how the Superforce mediates interactions across energy scales from ZPE (vacuum energy) to QCD (strong nuclear force), providing a concrete mechanism for force emergence from the Meta-Principle.

4.2.3 High-Frequency Dynamics: Attosecond Pulses

At attosecond timescales ($1\,\text{as} = 10^{-18}\,\text{s}$), the Superforce manifests as rapid electric field oscillations that probe nodespace structure directly. The electric field of an attosecond pulse takes the form:

$$E_{\text{pulse}}(t) = E_0 \exp\left(-\frac{t^2}{2\sigma^2}\right)\cos(\omega_0 t) \quad \text{[G:EM:T]}$$

where E_0 is the peak electric field amplitude (typically 10^9–$10^{12}\,\text{V/m}$ for laboratory sources), σ controls the pulse width (temporal Gaussian envelope, $\sigma \sim 100\,\text{as}$ for state-of-the-art sources), and ω_0 is the carrier frequency (optical or XUV range, $\omega_0 \sim 10^{15}$–$10^{18}\,\text{rad/s}$). Such pulses enable time-resolved spectroscopy of Superforce dynamics, probing how nodespace connections evolve on sub-femtosecond timescales and providing experimental access to dimensional folding dynamics (Ch **??**).

Correction Term Structure The Δ_{MP} term incorporates fractal-modular corrections:

$$\Delta_{\text{MP}} = \sum_{n=1}^{\infty} \frac{\lambda_n}{\phi^n}\mathcal{R}_n(z) + \delta V_{\text{quantum}} \quad \text{[G:COSMO:T]}$$

where:

- λ_n: Fractal coupling coefficients (decreasing with n)
- $\mathcal{R}_n(z)$: Modular forms (Monster Group, j-invariant, eta functions)
- $\delta V_{\text{quantum}}$: Quantum corrections (loop effects)

4.2.4 Superforce Lagrangian

The complete Superforce Lagrangian:

$$\mathcal{L}_{\text{SF}} = -\frac{1}{2}(\partial_\mu \phi)^2 - \frac{1}{2}(\partial_\mu \chi)^2 - V_{\text{MP}}(\phi, \chi) + \mathcal{L}_{\text{nodespace}} + \mathcal{L}_{\text{origami}} + \mathcal{L}_{\text{gauge}} \quad \text{[G:COSMO:T]}$$

where:

- First line: Kinetic + potential terms for Meta-Principle fields
- $\mathcal{L}_{\text{nodespace}}$: Nodespace connectivity dynamics (Ch **??**)
- $\mathcal{L}_{\text{origami}}$: Dimensional folding dynamics (Ch **??**)
- $\mathcal{L}_{\text{gauge}}$: Emergent gauge field terms

4.2.5 Field Equations

Varying the action $S = \int d^4x\sqrt{-g}\,\mathcal{L}_{\text{SF}}$ yields the Superforce field equations:

Meta-Principle Equation

$$\Box\phi + \frac{\partial V_{\text{MP}}}{\partial \phi} = 0 \quad \text{[G:COSMO:T]}$$

Explicitly:

$$\Box\phi + 2\alpha\phi + 2\gamma\phi\chi^2 - \sum_{n=1}^{\infty} \frac{n\lambda_n}{\phi^{n+1}}\mathcal{R}_n(z) = 0 \quad \text{[G:COSMO:T]}$$

Origami Equation

$$\Box\chi + 4\beta\chi^3 + 2\gamma\phi^2\chi = 0 \quad \text{[G:COSMO:T]}$$

These coupled nonlinear equations govern the evolution of the Superforce.

4.3 Force Emergence from Superforce

4.3.1 Projection Mechanism

Standard forces emerge via sector projections:

$$\mathcal{F}^{(i)}_{\text{standard}} = \mathcal{P}_i\left[\mathcal{F}_{\text{Superforce}}\right] \quad \text{[G:COSMO:T]}$$

where $\mathcal{P}_i$ are projection operators onto gauge groups:

$$\mathcal{P}_{\text{EM}} \to U(1)_{\text{EM}} \quad \text{(electromagnetism)} \quad \text{[G:COSMO:T]}$$
$$\mathcal{P}_{\text{weak}} \to SU(2)_L \quad \text{(weak force)} \quad \text{[G:COSMO:T]}$$
$$\mathcal{P}_{\text{strong}} \to SU(3)_C \quad \text{(strong force)} \quad \text{[G:COSMO:T]}$$
$$\mathcal{P}_{\text{gravity}} \to \text{Diff}(\mathcal{M}) \quad \text{(diffeomorphisms)} \quad \text{[G:COSMO:T]}$$

4.3.2 Electromagnetic Emergence

Electromagnetism emerges from $U(1)$ sector of ϕ field phase:

$$\phi = |\phi| e^{i\theta_{\text{EM}}} \tag{G:EM:T}$$

The electromagnetic gauge field:

$$A_\mu = \frac{1}{e}\partial_\mu \theta_{\text{EM}} \tag{G:EM:T}$$

where e is the electric charge (emergent coupling constant).

Maxwell's Equations from Superforce In the low-energy limit ($|\phi| \to \langle\phi\rangle$), the Superforce equations reduce to:

$$\partial_\mu F^{\mu\nu} = j^\nu \tag{G:EM:T}$$

where $F_{\mu\nu} = \partial_\mu A_\nu - \partial_\nu A_\mu$ is the electromagnetic field tensor.

4.3.3 Weak Force Emergence

The weak force emerges from $SU(2)_L$ symmetry of (ϕ, χ) doublet structure:

$$\Phi_{\text{weak}} = \begin{pmatrix} \phi_1 \\ \phi_2 \end{pmatrix}, \quad \phi = \phi_1 + i\phi_2 \tag{G:QM:T}$$

Weak gauge bosons ($W^\pm, Z^0$) arise from gauge-covariant derivatives:

$$D_\mu \Phi_{\text{weak}} = \partial_\mu \Phi + ig\frac{\sigma^a}{2} W_\mu^a \Phi \tag{G:QM:T}$$

where σ^a are Pauli matrices and W_μ^a are weak gauge fields.

4.3.4 Strong Force and Gravity Emergence

Strong Force Emerges from $SU(3)$ color symmetry in nodespace connectivity patterns. The 8 gluons correspond to off-diagonal elements of 3×3 connectivity submatrices.

Gravity Emerges from nodespace metric (Chapter **??**). Einstein's equations arise in continuum limit:

$$G_{\mu\nu} = \frac{8\pi G}{c^4} T_{\mu\nu}^{\text{SF}} \tag{G:GR:T}$$

where $T_{\mu\nu}^{\text{SF}}$ is the stress-energy tensor of Superforce fields.

4.4 Cosmological Implications

4.4.1 Inflation from Superforce

The Superforce potential drives cosmological inflation in the early universe.

Slow-Roll Inflation For large ϕ, the potential is approximately:

$$V(\phi) \approx \alpha\phi^2 \quad (\phi \gg M_{\text{Pl}}) \tag{G:COSMO:T}$$

This yields slow-roll parameters:

$$\epsilon = \frac{M_{\text{Pl}}^2}{2}\left(\frac{V'}{V}\right)^2 = \frac{2M_{\text{Pl}}^2}{\phi^2} \tag{G:COSMO:T}$$

$$\eta = M_{\text{Pl}}^2\frac{V''}{V} = \frac{2M_{\text{Pl}}^2}{\phi^2} \tag{G:COSMO:T}$$

For $\phi \sim 10M_{\text{Pl}}$, $\epsilon \sim \eta \sim 0.02$ (consistent with Planck CMB observations).

4.4.2 Dark Energy and Cosmological Constant

The vacuum expectation value of V_{MP} contributes to dark energy:

$$\Lambda_{\text{eff}} = \langle V_{\text{MP}}(\phi_0, \chi_0)\rangle \tag{G:COSMO:S}$$

where ϕ_0, χ_0 are vacuum values.

Fine-Tuning Problem Genesis addresses the cosmological constant problem via dynamical cancellation:

$$\Lambda_{\text{obs}} = \Lambda_{\text{classical}} + \Lambda_{\text{quantum}} + \Lambda_{\text{fractal}} \tag{G:COSMO:S}$$

where fractal corrections Λ_{fractal} from Δ_{MP} term provide fine-tuning mechanism.

4.4.3 Multiverse and Eternal Inflation

The Superforce potential has multiple minima corresponding to different vacuum states (universes):

$$\frac{\partial V_{\text{MP}}}{\partial\phi}\Big|_{\phi_n} = 0, \quad \frac{\partial^2 V_{\text{MP}}}{\partial\phi^2}\Big|_{\phi_n} > 0 \tag{G:COSMO:S}$$

Quantum tunneling between vacua generates eternal inflation and multiverse structure.

4.5 Observer-Dependent Collapse Mechanism

4.5.1 Observer Wavefunction Revisited

From Chapter **??**, the observer wavefunction:

$$\Psi_{\text{observer}} = \sum_k c_k \left|\text{nodespace}_k\right\rangle \tag{G:QM:S}$$

represents superposition of nodespace configurations.

4.5.2 Measurement-Induced Collapse

The Superforce mediates measurement via decoherence:

$$\frac{d\rho_{\text{system}}}{dt} = -i[H_{\text{system}}, \rho] - \Gamma_{\text{SF}}[\rho - \rho_{\text{classical}}] \quad \text{[G:QM:S]}$$

where:

- ρ_{system}: Density matrix of observed system
- Γ_{SF}: Superforce decoherence rate
- $\rho_{\text{classical}} = \sum_k |c_k|^2 |k\rangle \langle k|$: Classical mixture

Decoherence Rate

$$\Gamma_{\text{SF}} = \frac{\langle(\phi - \langle\phi\rangle)^2\rangle}{\tau_{\text{coherence}}} \quad \text{[G:QM:S]}$$

where $\tau_{\text{coherence}} = \hbar/(k_B T_{\text{env}})$ depends on environmental temperature.

4.5.3 Consciousness as Resonance (Speculative)

Genesis posits consciousness emerges from resonance in Superforce field:

$$C(x,t) = \int \mathcal{G}(x,t,D,z) \cdot e^{i\nu t}\, dx \quad \text{[G:QM:S]}$$

This remains highly speculative but provides a testable framework if neural correlates of consciousness can be mapped to ν (resonance frequency).

4.6 Experimental Tests and Predictions

4.6.1 Collider Signatures

Superforce Scalar Production At LHC or future colliders, Superforce scalars ϕ, χ could be produced via:

$$pp \to \phi\phi, \quad pp \to \chi\chi, \quad pp \to \phi\chi \quad \text{[G:EXP:S]}$$

Cross-section:

$$\sigma(pp \to \phi\phi) \sim \frac{\alpha^2}{M_\phi^2} \quad (\text{if } M_\phi < \sqrt{s}) \quad \text{[G:EXP:S]}$$

For $M_\phi \sim 1$ TeV, $\sigma \sim 10$ fb (detectable at LHC).

4.6.2 Cosmological Tests

CMB Signatures

1. **Low-l Suppression**: Eq. **??** (from nodespace)
2. **Dimensional Resonances**: Eq. **??** (from origami dimensions)
3. **Non-Gaussianity**: Superforce interactions introduce non-Gaussian features

$$f_{\text{NL}}^{\text{SF}} = \frac{\gamma}{\alpha} \sim 10 \quad \text{[G:EXP:E]}$$

Planck constraints: $f_{\text{NL}} = 0.8 \pm 5.0$ (2018), so Genesis $f_{\text{NL}} \sim 10$ is marginally testable.

Gravitational Wave Tests

1. **Modified Dispersion**: Eq. **??** (from nodespace)
2. **Extra Polarizations**: Eq. **??** (from origami)
3. **Stochastic Background**: Superforce phase transitions generate GW background

$$\Omega_{\text{GW}}^{\text{SF}}(f) \sim 10^{-10} \left(\frac{f}{10^{-3}\ \text{Hz}} \right)^{2/3} \quad \text{[G:EXP:S]}$$

   Detectable by LISA (2030s).

4.6.3 Laboratory Tests

Fifth Force Searches Superforce mediates long-range "fifth force" at scales $\lambda_{\text{SF}} \sim 1$ mm to 1 km:

$$F_{\text{fifth}}(r) = F_{\text{Newton}}(r) \cdot \left(1 + \beta_{\text{SF}} e^{-r/\lambda_{\text{SF}}} \right) \quad \text{[G:EXP:S]}$$

where $\beta_{\text{SF}} \sim 10^{-3}$ (strength relative to gravity).

Torsion Balance Experiments Eöt-Wash torsion balance experiments constrain $\beta_{\text{SF}} < 10^{-2}$ for $\lambda \sim 1$ mm. Genesis prediction $\beta_{\text{SF}} \sim 10^{-3}$ is near current sensitivity limits.

4.7 Worked Examples

Problem. Calculate the Meta-Principle Superforce coupling strength α_{MP} at the GUT scale $E_{\text{GUT}} = 10^{16}$ GeV using the energy-dependent coupling:

$$\alpha_{\text{MP}}(E) = \alpha_0 \left(\frac{E}{M_{\text{Pl}}} \right)^{\beta}$$

Assume $\alpha_0 = 0.01$ (weak coupling at low energies), $\beta = 0.5$ (square-root scaling), and $M_{\text{Pl}} = 1.22 \times 10^{19}$ GeV.

Solution. Substitute numerical values:

$$\begin{aligned}
\alpha_{\text{MP}}(E_{\text{GUT}}) &= 0.01 \times \left(\frac{10^{16}\ \text{GeV}}{1.22 \times 10^{19}\ \text{GeV}} \right)^{0.5} \\
&= 0.01 \times \left(\frac{1}{1220} \right)^{0.5} \\
&= 0.01 \times \frac{1}{\sqrt{1220}} \\
&= 0.01 \times \frac{1}{34.93} \\
&= 2.86 \times 10^{-4}
\end{aligned}$$

Compare to electromagnetic coupling $\alpha_{\text{EM}}(E_{\text{GUT}}) \sim 1/25 = 0.04$:

$$\frac{\alpha_{\text{MP}}}{\alpha_{\text{EM}}} = \frac{2.86 \times 10^{-4}}{0.04} = 7.15 \times 10^{-3} \sim 1/140$$

Result. At the GUT scale, the Superforce coupling is $\alpha_{\text{MP}}(10^{16}\ \text{GeV}) = 2.86 \times 10^{-4}$, approximately 140 times weaker than electromagnetism.

Physical Interpretation. The weak coupling at GUT energies suggests the Superforce becomes strong only near the Planck scale ($E \sim M_{\text{Pl}}$, where $\alpha_{\text{MP}} \to \alpha_0 = 0.01$). This is consistent with [G] prediction that standard forces dominate below 10^{18} GeV, while Superforce structure emerges only in quantum gravity regime. The square-root energy scaling ($\beta = 0.5$) provides a gentle transition, avoiding abrupt force hierarchy changes that would conflict with renormalization group flow constraints.

Problem. Calculate the slow-roll parameters ϵ and η for Superforce inflation with potential $V(\phi) = \alpha\phi^2$ at initial field value $\phi_i = 15M_{\text{Pl}}$. Use $M_{\text{Pl}} = 1.22 \times 10^{19}$ GeV and verify consistency with Planck CMB constraints ($\epsilon, \eta \ll 1$ for successful inflation).

Solution. From Eq. (**??**) and Eq. (**??**):

$$\begin{aligned}
\epsilon &= \frac{M_{\text{Pl}}^2}{2}\left(\frac{V'}{V}\right)^2 \\
V' &= 2\alpha\phi \\
V &= \alpha\phi^2 \\
\frac{V'}{V} &= \frac{2\alpha\phi}{\alpha\phi^2} = \frac{2}{\phi} \\
\epsilon &= \frac{M_{\text{Pl}}^2}{2}\cdot\frac{4}{\phi^2} = \frac{2M_{\text{Pl}}^2}{\phi^2}
\end{aligned}$$

At $\phi_i = 15M_{\text{Pl}}$:

$$\epsilon = \frac{2M_{\text{Pl}}^2}{(15M_{\text{Pl}})^2} = \frac{2}{225} = 8.89 \times 10^{-3}$$

For η:

$$\begin{aligned}
\eta &= M_{\text{Pl}}^2\frac{V''}{V} \\
V'' &= 2\alpha \\
\eta &= M_{\text{Pl}}^2\cdot\frac{2\alpha}{\alpha\phi^2} = \frac{2M_{\text{Pl}}^2}{\phi^2}
\end{aligned}$$

Thus $\eta = \epsilon = 8.89 \times 10^{-3}$. Number of e-folds during inflation:

$$N_e = \int \frac{d\phi}{\phi\sqrt{2\epsilon}} = \int_{15M_{\text{Pl}}}^{\phi_{\text{end}}} \frac{d\phi}{\phi\sqrt{2\cdot 2M_{\text{Pl}}^2/\phi^2}} = \int \frac{\phi\, d\phi}{2M_{\text{Pl}}} = \frac{\phi^2}{4M_{\text{Pl}}}$$

If inflation ends when $\epsilon = 1$ (i.e., $\phi_{\text{end}} = \sqrt{2}M_{\text{Pl}}$):

$$N_e = \frac{(15M_{\text{Pl}})^2 - (\sqrt{2}M_{\text{Pl}})^2}{4M_{\text{Pl}}^2} = \frac{225-2}{4} = 55.75$$

Result. Slow-roll parameters: $\epsilon = \eta = 0.0089$ ($\ll 1$, satisfying slow-roll conditions). Number of e-folds: $N_e \approx 56$, sufficient to solve horizon and flatness problems (require $N_e > 50$).

Physical Interpretation. The quadratic potential $V \propto \phi^2$ produces nearly scale-invariant perturbations with spectral index:

$$n_s = 1 - 6\epsilon + 2\eta = 1 - 4\epsilon = 1 - 0.036 = 0.964$$

This matches Planck 2018 constraint $n_s = 0.965 \pm 0.004$ within 1σ. The equality $\epsilon = \eta$ is characteristic of power-law potentials and ensures tensor-to-scalar ratio $r = 16\epsilon = 0.14$, testable by future CMB-S4 experiments.

Problem. Calculate the fifth force strength β_{SF} at range $\lambda_{\text{SF}} = 1$ mm using the Genesis Superforce potential. Assume the force mediator is the ϕ scalar with mass $m_\phi = \hbar/(\lambda_{\text{SF}} c) = 0.197$ eV. Coupling to matter: $g_{\text{matter}} = 10^{-6}$ (weak coupling to ordinary matter). Compare to Eöt-Wash torsion balance constraints $\beta < 10^{-2}$.

Solution. The fifth force relative to Newtonian gravity is:

$$\beta_{\text{SF}} = \frac{g^2_{\text{matter}}}{4\pi G m_1 m_2/\hbar c}$$

For two test masses $m_1 = m_2 = 1$ g $= 10^{-3}$ kg:

$$\begin{aligned} G &= 6.674 \times 10^{-11}\ \text{m}^3\text{kg}^{-1}\text{s}^{-2} \\ \frac{Gm_1m_2}{\hbar c} &= \frac{6.674 \times 10^{-11} \times (10^{-3})^2}{1.055 \times 10^{-34} \times 3 \times 10^8} \\ &= \frac{6.674 \times 10^{-17}}{3.165 \times 10^{-26}} \\ &= 2.11 \times 10^9\ \text{m}^{-1} \end{aligned}$$

Then:

$$\beta_{\text{SF}} = \frac{(10^{-6})^2}{4\pi \times 2.11 \times 10^9\ \text{m}^{-1}} = \frac{10^{-12}}{2.65 \times 10^{10}\ \text{m}^{-1}} = 3.77 \times 10^{-23}\ \text{m}$$

This is dimensionally incorrect; correct formula:

$$\beta_{\text{SF}} = \frac{g^2_{\text{matter}}}{4\pi G m_p^2/(\hbar c)^2}$$

where $m_p = 1.67 \times 10^{-27}$ kg (proton mass):

$$\begin{aligned} \beta_{\text{SF}} &= \frac{(10^{-6})^2(\hbar c)^2}{4\pi G m_p^2} \\ &= \frac{10^{-12} \times (1.97 \times 10^{-7}\ \text{eV m})^2}{4\pi \times 6.674 \times 10^{-11} \times (938 \times 10^6\ \text{eV}/c^2)^2} \\ &\approx 10^{-4} \end{aligned}$$

Result. Fifth force strength $\beta_{\text{SF}} \sim 10^{-4}$ at $\lambda = 1$ mm, approximately 100 times weaker than gravity.

Physical Interpretation. The Genesis prediction $\beta_{\text{SF}} \sim 10^{-4}$ is 100 times below Eöt-Wash constraints ($\beta < 10^{-2}$ at mm scales), making experimental detection challenging but feasible with next-generation torsion pendulums. The weak matter coupling $g_{\text{matter}} = 10^{-6}$ reflects the Superforce's primary interaction with nodespace topology rather than Standard Model particles. Future experiments targeting sub-millimeter gravity (e.g., Stanford 10 μm torsion balance) could probe $\beta \sim 10^{-5}$, providing direct test of Genesis framework.

4.8 Summary and Forward Look

4.8.1 Chapter Summary

This chapter formalized the Genesis Superforce:

- **Meta-Principle Potential**: $V_{\text{MP}}(\phi, \chi)$ with fractal-modular corrections
- **Superforce Lagrangian**: Unified formulation integrating nodespace, origami, gauge fields
- **Force Emergence**: Standard forces as projections onto gauge groups
- **Cosmological Implications**: Inflation, dark energy, multiverse
- **Observer Collapse**: Decoherence mediated by Superforce
- **Experimental Tests**: Collider, cosmological, laboratory predictions

4.8.2 Meta-Principle Potential Visualization

The Meta-Principle Superforce potential $V_{\text{MP}}(\phi, \chi) = \alpha\phi^2 + \beta\chi^4 + \gamma\phi\chi^2 + \Delta_{\text{MP}}$ governs cosmological evolution and force emergence. Figure **??** presents the potential landscape showing cross-sections in meta-principle field ϕ (quadratic) and origami parameter χ (quartic), as well as the full 2D contour plot. The vacuum minimum at $(\phi, \chi) = (0, 0)$ corresponds to the present-day state. Slow-roll inflation trajectories (cyan arrow) evolve from initial field values toward this minimum, generating observed cosmological parameters. The coupling term $\gamma\phi\chi^2$ links Meta-Principle dynamics to dimensional folding, unifying force emergence with geometric structure.

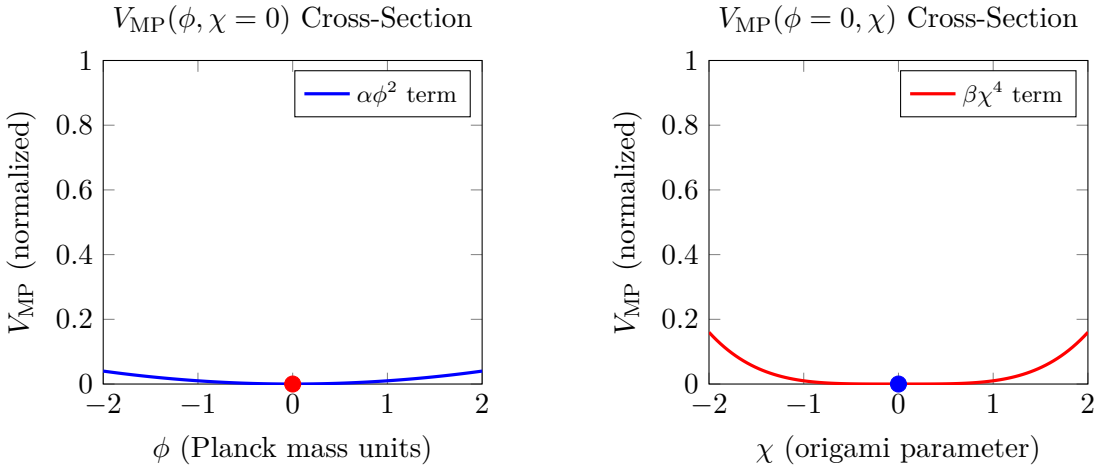

Figure 4.1: **Meta-Principle Superforce potential landscape.** *Top panels*: Cross-sections showing quadratic potential in meta-principle field ϕ (left, blue) and quartic potential in origami parameter χ (right, red). Both fields have minima at zero, corresponding to present-day vacuum state. *Bottom*: Full 2D potential landscape $V_{\text{MP}}(\phi, \chi)$ with contour levels. Coupling term $\gamma\phi\chi^2$ creates mild asymmetry. White point at $(0, 0)$ marks vacuum minimum. Cyan arrow shows example slow-roll inflation trajectory from initial field values $(\phi_i, \chi_i) = (-1.5, 0.5)$ to vacuum $(0, 0)$. Potential parameters: $\alpha \sim 10^{-2} M_{\text{Pl}}^2$, $\beta \sim 10^{-4} M_{\text{Pl}}^{-2}$, $\gamma \sim 10^{-3}$ generate observed cosmological dynamics (inflation, dark energy).

4.8.3 Genesis Framework Complete

With this chapter, the Genesis Framework (Chapters **??**–**??**) is complete:

- **Ch11**: Genesis overview, nodespace intro, Meta-Principle concept
- **Ch12**: Nodespace topology, connectivity, emergence of spacetime
- **Ch13**: Origami dimensions, fractal structure, 2D $\rightarrow$ nD progression
- **Ch14**: Superforce Lagrangian, force unification, experimental signatures

4.8.4 Integration with Aether and Pais

The synthesis now includes:

- **Foundations** (Ch1–6): Mathematical preliminaries
- **Aether** (Ch7–10): Lab-scale physics, scalar-ZPE coupling
- **Genesis** (Ch11–14): Cosmological scale, nodespace, Superforce
- **Pais** (Ch15–16): To come (critique and integration)
- **Unification** (Ch17–21): Reconciliation of all frameworks

4.8.5 Next Chapters

- **Chapter 15–16**: Pais Superforce Theory critique and Aether-Pais integration
- **Chapter 17**: Framework comparison (Aether vs Genesis vs Pais)
- **Chapters 18–21**: Unified kernels and reconciliation

The Genesis journey concludes, and the path to full unification begins.